DESIGN OF A LARGE-SCALE DETONATION TUBE

A Thesis

by

MATTHEW THOMAS GILL

Submitted to the Office of Graduate and Professional Studies of
Texas A&M University
in partial fulfillment of the requirements for the degree of

MASTER OF SCIENCE

Chair of Committee,	Eric L. Petersen
Committee Members,	Chad V. Mashuga
	Timothy J. Jacobs
Head of Department,	Andreas A. Polycarpou

May 2016

Major Subject: Mechanical Engineering

ABSTRACT

Multiple vital industries, especially those in the energy sector, are vulnerable to unexpected detonation events. Extremely destructive and difficult to predict, the processes by which they are formed and the limits over which they can propagate have been a significant focus of research for years, but it is often difficult to carry out relevant experiments on any significant scale. This work presents the motivations for such study, the basic theory required to understand what is happening within a detonation, and the designs for a proposed facility which could be used to broaden the scope of current detonation research. It would allow the detonation phenomenon to be studied at a scale which is rarely achievable and with a precision which is rarely accomplished. This would help to either validate or disprove trends which have been established with small-scale rigs but not tested at the proposed size.

Most detonation tubes have diameters no larger than a 30 cm; the proposed facility boasts an internal diameter of 70 cm and a length of 100 m, allowing mixtures which are usually outside of the range of detonation to be studied in novel ways. Detonations can be induced through deflagration-to-detonation transition using a small point energy source, or directly initiated via a shock wave or the explosion of a separate, more energetic mixture. Measurement is accomplished with pressure transducers and photodiodes spaced down the length of the tube. End-tube diagnostics include fast-framing Schlieren imaging and Planar Laser-Induced Fluorescence, and use elongated windows to view the tube interior, allowing the reaction zone structure to be studied at large scale. Smaller windows spaced down the length of the tube enable additional data-gathering capabilities where

necessary. The implementation of this facility would serve to increase the scope of understanding of detonation events and contribute to the improvement of safety standards for vulnerable workplaces.

ACKNOWLEDGMENTS

NOMENCLATURE

ASME American Society of Mechanical Engineers

BPVC Boiler and Pressure Vessel Code

BR   Blockage Ratio

CJ   Chapman-Jouguet

DDT   Deflagration-to-Detonation Transition

FEA   Finite Element Analysis

GETF Gas Explosion Test Facility

NIOSH National Institute for Occupational Health and Safety

PLIF   Planar Laser Induced Fluorescence

VCE   Vapor Cloud Explosion

ZND   Zeldovich-Von Neumann-Döring

A   Correlation constant for cell size determination

c   Speed of sound

C_P Constant pressure specific heat

D   Velocity of combustion wave or internal tube diameter

D_i Internal tube diameter

h   Specific enthalpy

K   Variable introduced to simplify Rankine-Hugoniot notation

l Reaction zone length

L   Detonation cell length

M   Mach number

$\dot{m}$	Mass flux
O	Order of
P	Static pressure
Q	Heat of reaction
S	Variable introduced to simplify Rankine-Hugoniot notation
T	Temperature
t	Tube wall thickness
u	Flow velocity
x	Ratio of product to reactant specific volume
y	Ratio of product to reactant pressure
α	Variable introduced to simplify Hugoniot Curve notation
β	Variable introduced to simplify Hugoniot Curve notation
η	Function of wave velocity introduced to simplify notation
γ	Ratio of specific heats
λ	Detonation cell size
ν	Specific volume
ρ	Density
$_0$	Property of reactant, or upstream, flow
$_1$	Property of product, or downstream, flow
*	Property of Chapman-Jouguet condition
$'$	Value relative to stationary coordinate system
$_{Det}$	Pertaining to detonation solution

f	Formation
H	Pertaining to the Hugoniot Curve
R	Pertaining to the Rayleigh Line
s	Isentropic
T	Total
VN	Von Neumann

TABLE OF CONTENTS

LIST OF FIGURES

1. INTRODUCTION

Detonation Hazards

The energy industry is vital to the maintenance of the modern standard of living, but many of the facilities essential to energy production are accompanied by some risks which must be mitigated. Although many are built securely enough to withstand deflagration processes, few can withstand the significant overpressures caused by detonations. Because of this, it is essential to build the facilities so that detonation is extremely unlikely, and to predict the conditions under which it could occur.

Models exist which can predict detonation limits, the concentrations of fuel which can potentially detonate given a proper ignition source, but most of the research done to validate these models has focused on the smaller scale. This thesis contains designs for a detonation tube on a much larger scale than is usually seen. The intent is to build it at the Riverside campus of Texas A&M University, due to the strategic combination of well-suited land, academic prowess, and proximity to industrial centers such as Houston.

Reaching a greater understanding of the scaling behavior of the detonation process is important in order to improve the safety of the industry. The two industrial sectors which initially generated this interest are petrochemical facilities and coal mines.

Petrochemical Facility Risks

In December of 2005, a detonation wave destroyed the majority of the Buncefield fuel reserve at Hertfordshire, England, which at the time supplied over half of the daily

1

fuel used by Heathrow airport. No previously conducted hazard analysis had revealed a threat of detonation, but when winter-grade gasoline leaked from a storage tank, became entrained with air, and ignited, the damage left by the blast showed signs of overpressures characteristic of a detonation wave. Research conducted after the incident revealed that as the initial deflagration wave passed through a stand of trees, the branches generated turbulence. This increased the surface area of the wave front, causing the rate of reaction to increase and allowing the deflagration wave to accelerate until it became a detonation wave [1-4].

This event is known as a vapor cloud explosion (VCE), and it is not unique to Buncefield. Similar disasters have occurred in Jaipur, India; Saint-Herblain, France; Naples, Italy; and Newark, New Jersey [5]. Under certain conditions, detonation can even occur without the presence of a leak [6]. Taken as a whole, these events have exacted a heavy cost in the form of both human casualties and property damage.

Coal Mine Risks

While petrochemical plants are mostly safe from detonation unless volatile compounds escape, coal mines are inherently vulnerable. The process of mining generates coal dust and releases natural gas. If an ignition source is present, along with the correct concentration of fuel and oxidizer, deflagration could be the result. The supports which prevent the tunnels from collapsing can generate enough turbulence to cause sufficient acceleration to result in a transition to detonation, a process known as Deflagration to Detonation Transition (DDT). Between 1976 and 2010, explosions formed in this manner

killed 186 coal miners in the USA and injured many more [7]. Needless to say, it is important to understand how DDT and VCE's can be prevented, or at least arrested if initiated [8-12].

Academic Interest

In addition to the concern for increased workplace safety, the detonation tube would increase the body of knowledge surrounding detonation limits and reaction zone structures. The study of detonation limits encompasses the mixtures, gas states, geometries, and ignition energies which could allow a detonation wave to be formed [13]. Models exist to predict this likelihood, but they have been difficult to verify experimentally at large diameters as most existing detonation tubes have relatively small internal diameters (on the order of 1.3 mm to 30 cm)[14, 15]. A larger tube would allow for experimentation that could be used to refine the models.

The study of the reaction zone structure involves the examination of the geometry of the detonation front itself. This type of study is difficult due to the speed at which the detonation wave moves, but it has been accomplished by several researchers through a combination of schlieren imaging, Planar Laser Induced Fluorescence (PLIF), and chemiluminescence [16-18]. The observations were, again, induced at a small scale. It is assumed that the behaviors found at this scale could be extrapolated out to the large scale, but it has yet to be verified.

3

Suitability of Texas A&M

Texas A&M University (TAMU) is well-suited for this project. In addition to the academic capabilities located there, it also has access to a separate campus, referred to as the Riverside campus, located roughly ten miles away from the flagship location. It has the space to accommodate a large experimental apparatus, an infrastructure to supply it and the researchers who would operate it, and is sufficiently distant from populated areas that the loud noises that the tests will cause are allowable. The location is also relatively close to Houston, a city with significant oil industry presence and the manufacturing capabilities to supply it. This proximity would reduce the costs of building the tube and allow for faster response for modifications and repairs.

Outline

This thesis covers previous works which have informed the current design, followed by detonation theory, including how to characterize expected detonation and deflagration behavior based on initial conditions. Detonation structures, the transition process between deflagration and detonation, and diagnostic techniques are also discussed.

The proposed designs of the facility are then described, with particular attention given to the decision and analysis processes behind each design choice. The suggested operational procedure is then described.

2. RELATED WORK

Gas Explosion Test Facility

The most similar facility to the proposed detonation tube was the Gas Explosion Test Facility (GETF) built at Lake Lynn, Pennsylvania for the National Institute for Occupational Safety and Health (NIOSH). The tube was used to study natural gas explosions in coal mines, which occur after the natural gas seeps in through cracks in the walls and gathers in inactive regions of the tunnels [19]. Following this event, ignition could occur and develop into detonation, which was the cause of several mine explosions.

To further investigate coal mine-related explosions, a large detonation tube was built. It was 73 meters long, with an internal diameter of 1.05 meters. Constructed from 12 meter-long sections of hot-rolled structural steel of thickness 9.5 mm and minimum yield strength of 248 MPa, it was calculated to have a factor of safety of 2.7, given the expected pressures produced from stoichiometric natural gas-air mixtures in a quasi-static Chapman-Jouguet (CJ) detonation process. Ignition was achieved via spark or by a bag filled with a mixture of CH_4 and O_2, and a system of pipes and a blower fan was used to circulate the mixture within the tube prior to ignition. Diagnostics consisted of 23 pressure transducers and 23 light emission sensors. The detonation structure was studied through the use of smokefoils—metal plates covered in soot from a kerosene flame which show distinct patterns after the passage of a detonation wave. Baffles constructed from horizontal I-beams within the tube were used as obstructions to study the DDT process [19].

The detonation tube was effectively open at one end, emitting a large quantity of supersonic gas with each test and producing a significant amount of noise. A curved ramp was installed at the end of the tube to redirect the flow upwards. After some use, the facility was upgraded with a "silencer" consisting of a grid of I-beams at the exit of the tube, and a grate was attached to the end to discourage wildlife from nesting inside [19]. Figure 1 shows the main features of the tube ignition section, main length, and exhaust end.
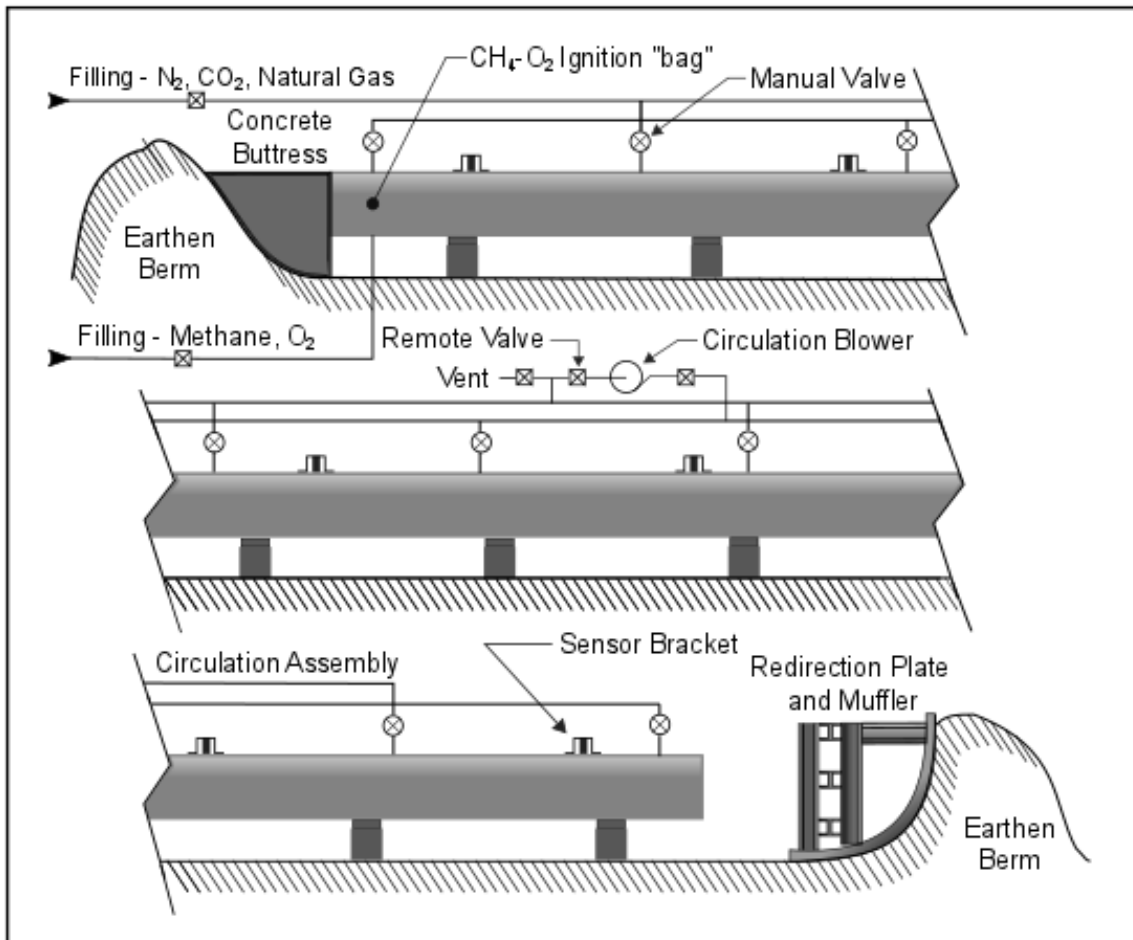
Figure 1. Diagram of NIOSH Gas Explosion Test Facility in PA [19].

The tube was used to study methane-oxygen mixtures and the detonation structures that they caused. The facility was built in 2008 but was dismantled in 2012. It was used to study mixtures that could form detonations in the established geometry, the length of the reaction zone, detonation velocities, and detonation cell size [7, 19, 20].

Reaction Zone PLIF

PLIF is a diagnostic technique which is very well-suited to detonation wave research. A series of lenses converts a laser beam from a single line into a sheet, which then passes through a fluid medium. If the frequency of the laser matches one of the energy level transitions available to at least one species of the gas mixture, it will fluoresce, and a camera positioned perpendicularly to the sheet can be used to record the emission along the plane. From this data, measurements of temperature, pressure, velocity, and concentration can be determined. A rapid-response technique such as this is ideal for a process which occurs as quickly as detonation waves do, and the planar nature of the data is well-suited to the analysis of transient structures such as those which make up the detonation front. A simplified diagram of a PLIF setup is shown in Figure 2.
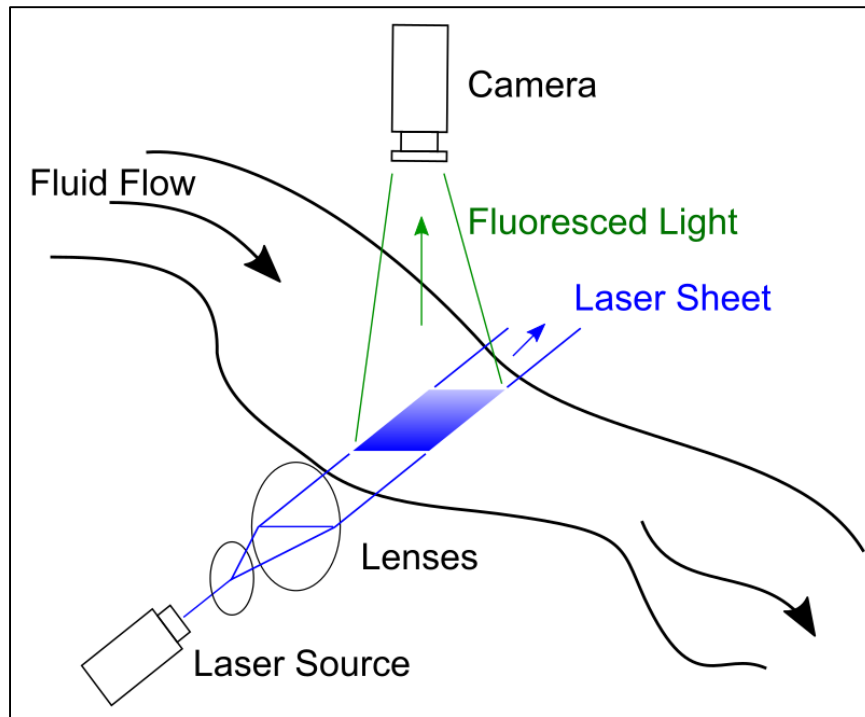
Figure 2. Simplified diagram of PLIF equipment setup.

Schlieren diagnostics use a light source spread by a slit and knife edge to examine density gradients in a fluid cross-section. The beam of light is made parallel by lenses or mirrors and passed through the medium, where density gradients cause varying degrees of refraction. The resulting image can be used to visualize the flow field. A simplified schlieren setup is shown in Figure 3.
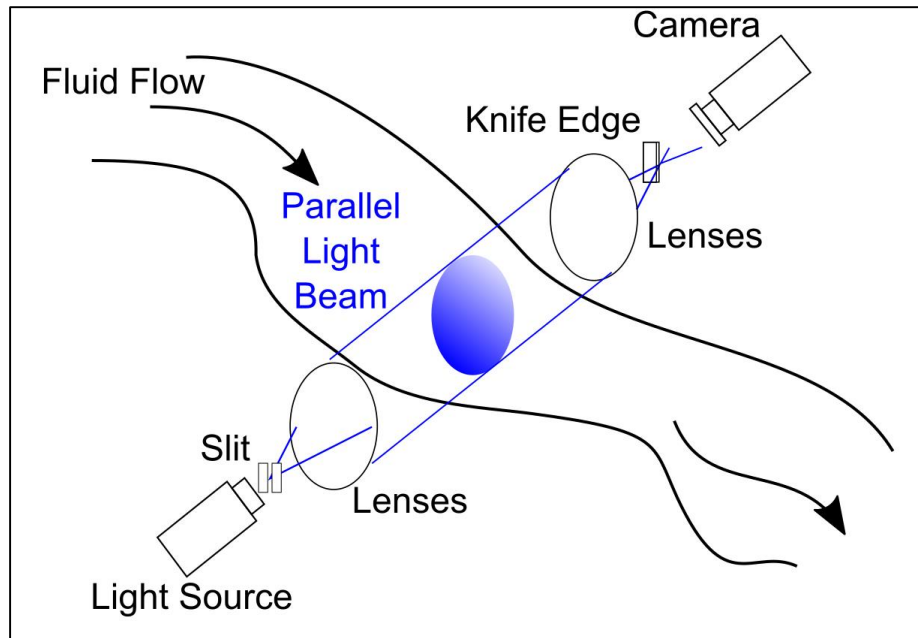
Figure 3. Simplified diagram of schlieren setup.

The California Institute of Technology and the University of Science and Technology of China have used PLIF to study the structure of the reaction zone in a small channel (152x18mm) and a small shock tube (13 cm internal diameter), respectively [16-18]. The techniques were combined with schlieren imaging and chemiluminescence. The structure for large-scale detonation has been studied using smoke foils, but not using these imaging techniques.

3. THEORY

Combustion Wave Basics

     This work is primarily concerned with combustion waves occurring in premixed gaseous media containing some combustible mixture. If the mixture and thermodynamic state are conducive to combustion and a sufficient amount of energy is introduced to initiate the event, the reaction begins and propagates away from the point of ignition [13]. The manner in which this occurs varies greatly from process to process; the reaction could be laminar or turbulent, subsonic or supersonic, and can be affected by many other factors, but it is often convenient to simplify the analysis by considering the wave to be a unidimensional structure as shown in Figure 4.
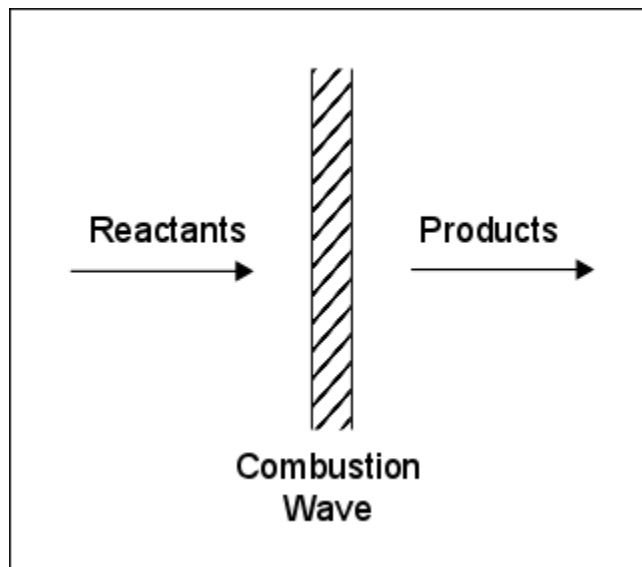
Figure 4. One-dimensional combustion wave diagram with wave-fixed coordinates.

Reactants which enter the combustion wave are heated until they reach the point of combustion, then react and produce high-temperature products. The release of chemical energy then sustains the wave [13].

Detonations versus Deflagrations

The two general types of self-sustaining combustion events are deflagrations and detonations. Deflagrations propagate at subsonic velocities, and so can be affected by disturbances before or after the wave. Energy transfer occurs via diffusion from the high-temperature products to the reactants, initiating the reaction that sustains the deflagration. Furthermore, they are inherently unstable [13]. A simplified deflagration structure is shown in Figure 5.
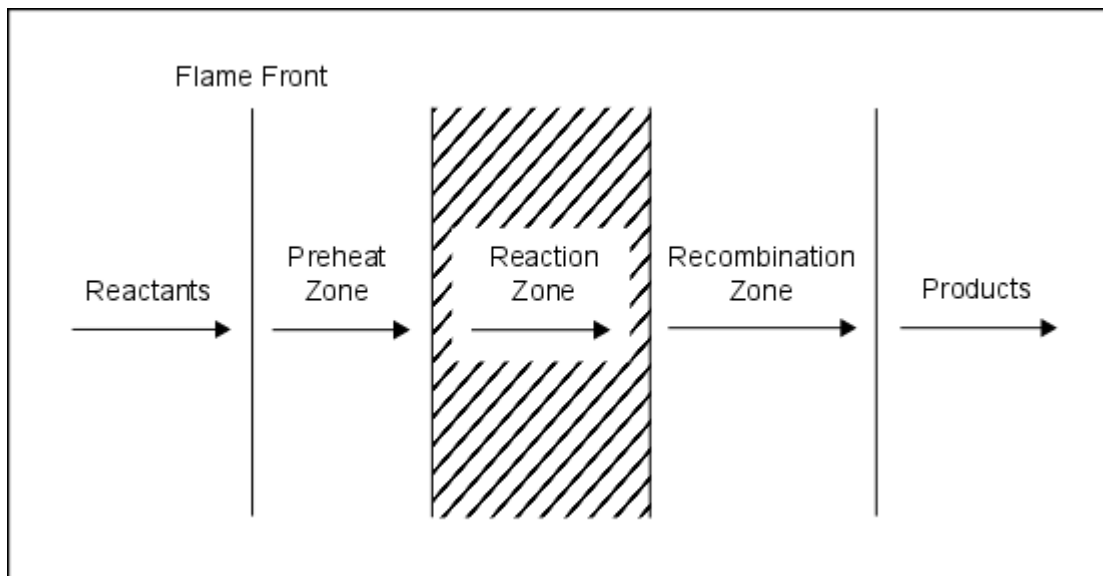
Figure 5. Diagram of deflagration wave structure with wave-fixed coordinates.

Detonations propagate at supersonic velocities, and while they are intrinsically unstable, they can often be treated as a precursor shock wave followed by a reaction zone, where the energy release required to sustain the shock wave occurs. This difference in propagation mechanism results in stark differences between the effects of the two types of combustion waves. Detonation waves are often modeled using the ZND (Zeldovich-Von Neumann-Döring) model, which treats the system as a shock wave followed by a reaction zone. The two are distinct, as shown in Figure 6.
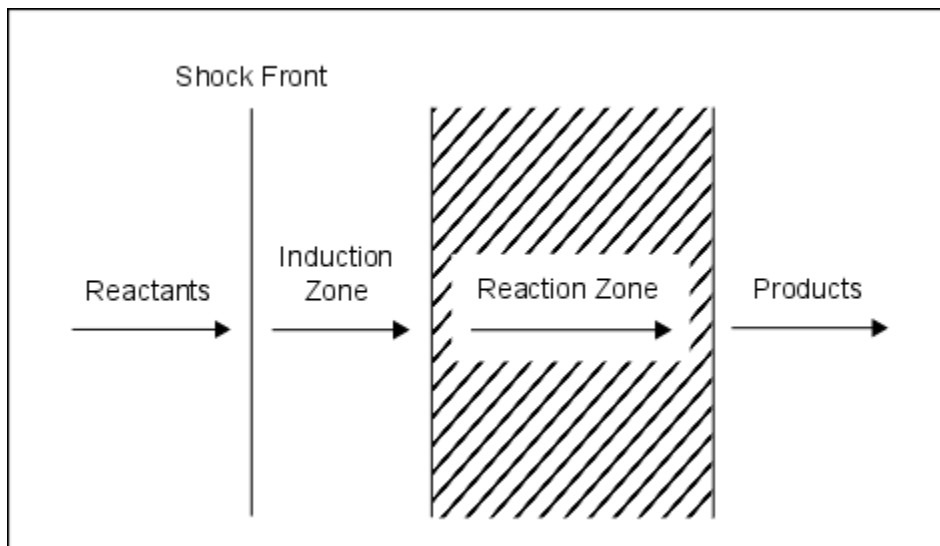
Figure 6. Diagram of detonation wave structure as described by ZND model.

The initial pressure and temperature changes occur over a distance on the order of a few mean free paths of the molecules, and can be considered instantaneous for the purposes of most calculations. The pressure decays after this point until it reaches that of the reaction zone. The relative widths of the different sections are not to scale in the figure,

as it was constructed to emphasize the distinction between the shock wave and reaction zone.

To summarize, detonation waves propagate faster than deflagration waves (at supersonic velocities), cause significant gas compression, are formed from a coupled shock front and reaction zone, and cause ignition of the unreacted gas via the temperature rise caused by the leading shock wave.

Deflagration waves, by contrast, usually propagate at subsonic velocities, cause gas expansion, are formed from preheating, reaction, and recombination zones, and cause ignition via diffusive heat transfer from the products to the reactants [13].

Basic Equations

Analysis of the simplified combustion wave begins with the continuity, conservation of momentum, and conservation of energy equations. They are applied across the combustion wave with wave-fixed coordinates and do not assume that the wave is a discontinuity (as in the shock wave leading a detonation). In fact, the initial analysis ignores the structure of the wave entirely, only taking into account what enters and what leaves. The notation to be used is shown in Figure 7 and Figure 8 .
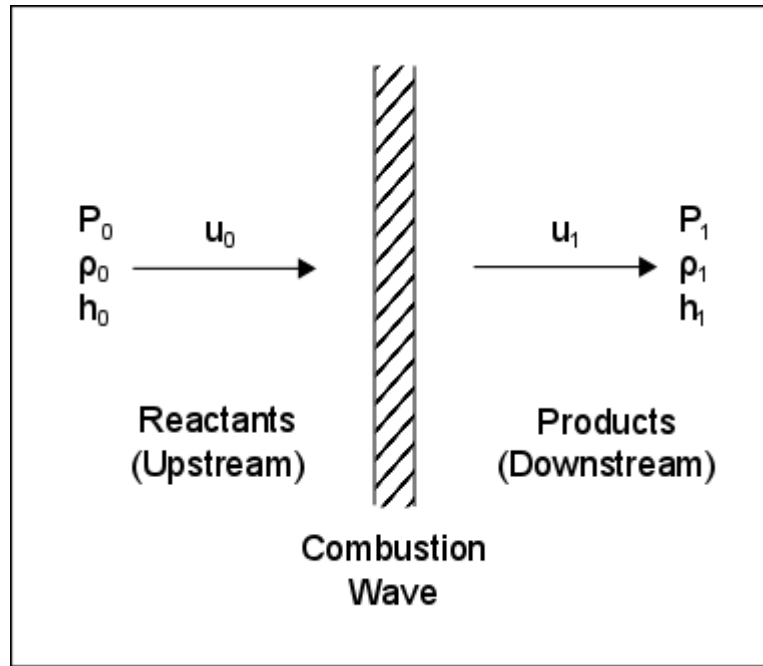
Figure 7. Combustion wave schematic in wave-fixed coordinates.

Where $P, \rho, h,$ and u represent the static pressure, density, specific enthalpy, and velocity of the medium, and the subscripts 0 and 1 denote reactants and products, respectively. Figure 7 is drawn with wave-fixed coordinates, which are more useful for the initial calculations, but the goal will include variables in laboratory-fixed coordinates, as shown in Figure 8.
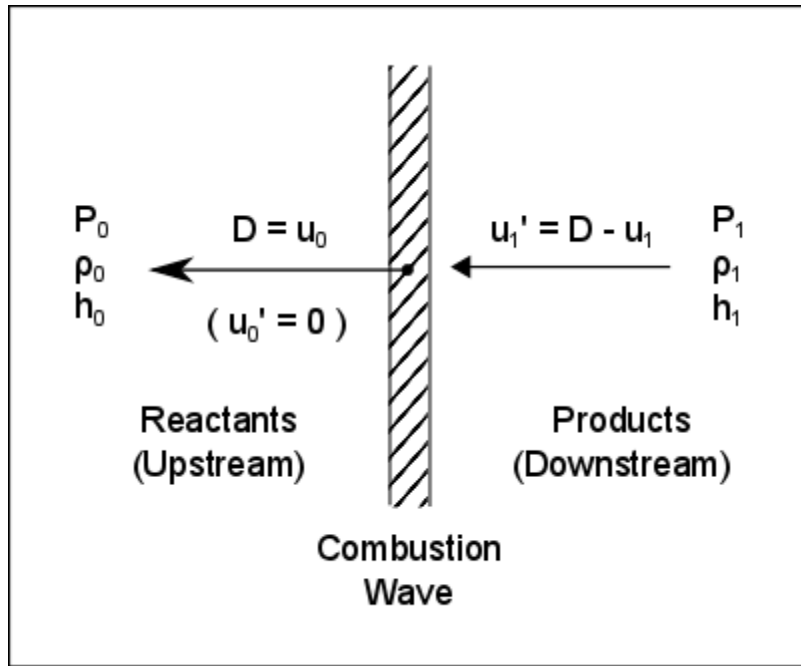
Figure 8. Combustion wave schematic with laboratory-fixed coordinates.

Where u_0' and u_1' represent the velocities of the reactants and products relative to a fixed coordinate system, respectively, and D represents the wave velocity. Because the wave is considered to be propagating into stationary reactants, the particle velocity u_0' is zero, and the wave velocity D and reactant particle velocity relative to the wave u_o have the same value. The wave induces movement in the products of velocity u_1' in the direction of the wave, which can be calculated from the wave velocity and flow velocity as shown in Figure 8. Given two of the three unique velocities (u_0, u_1, and u_1'), the third can be calculated.

The general calculation path to be followed is that of Lee [13]. As state variables in the reactants are much more easily measured, the unknown quantities to be evaluated

are those of the products (P_1, ρ_1, h_1) and the velocity information u_0 and u_1 (from which the wave velocity D and induced product velocity $u_1{}'$ can be determined. To do so will require five equations: the conservation of mass, momentum, and energy, as well as an equation of state and one additional criterion, the CJ criterion, which is explained later.

Values are evaluated far enough from the combustion wave that gradients in the reactants and products are relatively small. The form of the conservation of mass equation to be used is

$$\rho_0 u_0 = \rho_1 u_1 \tag{1}$$

the conservation of momentum equation is

$$P_0 + \rho_0 u_0^2 = P_1 + \rho_1 u_1^2 \tag{2}$$

and the conservation of energy equation is

$$h_0 + \frac{u_0^2}{2} = h_1 + \frac{u_1^2}{2} \tag{3}$$

where h, the specific enthalpy of the fluid, includes both formation and sensible enthalpy.

Rayleigh Line

The Rayleigh line combines the conservation of mass and conservation of momentum equations across the combustion wave to show pressure and specific volume ratios which are viable for combustion reactions. Combining Equations (1) and (2) yields

16

$$\frac{P_1 - P_0}{v_0 - v_1} = \rho_0^2 u_0^2 = \rho_1^2 u_1^2 = \dot{m}^2 \tag{4}$$

where v is the specific volume and $\dot{m}$ is the mass flux per unit of cross-sectional area of the fluid crossing the combustion wave. It is apparent from this that

$$\dot{m} = \sqrt{\frac{P_1 - P_0}{v_0 - v_1}} = \sqrt{\left(\frac{y-1}{1-x}\right)\frac{P_0}{v_0}} \tag{5}$$

where y and x are density and pressure ratios, respectively, defined as

$$y \equiv \frac{P_1}{P_0} \tag{6}$$

$$x \equiv \frac{v_1}{v_0} = \frac{\rho_0}{\rho_1} \tag{7}$$

These two variables define a plane on which the progress of the combustion reaction can take place, which is shown in Figure 9.
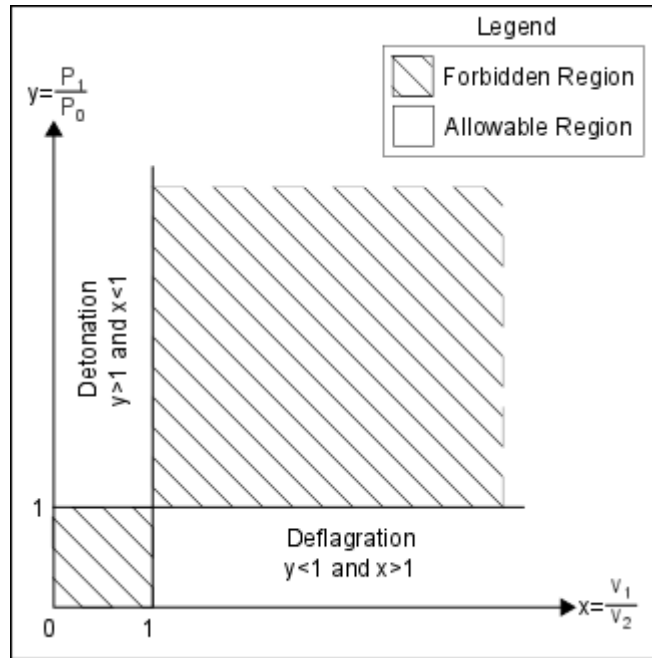
Figure 9. P-v ratio plane showing mathematically allowable combustion regions.

Only two regions are possible in this pane, those listed as deflagration and as detonation. From Equation (5), it is apparent that the numerator and denominator of the equation must either both be positive or both be negative for the mass flow rate to be real, so the shaded areas are impossible. Equation (5) also defines a line on the plane which satisfies the conservation of mass and of momentum, the Rayleigh line. It is fixed by two slopes (one each for the detonation and deflagration regions), and point (1,1), which it must contact to cross between the regions without entering the impossible zones. While the slope can be determined as a function of various quantities, it is convenient to do so in terms of the Mach number of the upstream flow, defined as

$$M_0 = \frac{u_0}{c_0} \tag{8}$$

where M is the Mach number and c is the speed of sound, calculated using

$$c = \sqrt{\gamma P v} \tag{9}$$

where γ is the ratio of specific heats. This equation does not require an equation of state to form. Combining Equations (5), (8), and (9) yields the slope of the Rayleigh line in terms of these quantities as

$$\frac{dy}{dx} = -M_0^2 \gamma_0 \tag{10}$$

This equation defines it with the addition of the point that it must pass through at point (1,1). The reason for the difference in slopes between the detonation and deflagration regions is that the Mach number should be less than one for deflagrations and greater than one for detonations. The Rayleigh Line is shown in Figure 10.
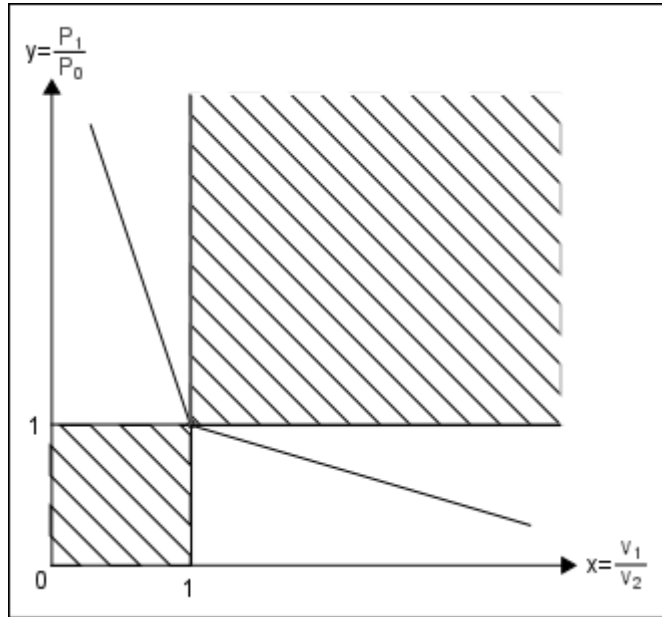
Figure 10. Rayleigh Line overlaid onto P-v ratio plane.

For later use, it is convenient to represent this line in another format. Equation (10) can be

manipulated into this form:

$$y = (1 + \gamma_0 M_0^2) - (\gamma_0 M_0^2)x \qquad (11)$$

Hugoniot Curve

The conservation of energy equation is now introduced in the form

$$h_{0_T} + \frac{u_0^2}{2} = h_{1_T} + \frac{u_1^2}{2} \qquad (12)$$

where h_{0_T} and h_{1_T} are enthalpy values including both formation and sensible enthalpy. It

is useful to separate these two values as

$$h_T = h_f^o + h \tag{13}$$

where h_f^o is formation enthalpy, and h is the sensible enthalpy. Sensible enthalpy is defined here as

$$h \equiv \int_{298}^{T} C_P dT \tag{14}$$

where C_P is the specific heat of the gas. This allows the heat of the reaction to be defined as

$$q \equiv \sum_{i}^{reactants} x_i h_{f\,i}^o - \sum_{j}^{products} x_j h_{f\,j}^o \tag{15}$$

and where q is the heat of reaction, and x_i is the mole fraction of component i of the mixture. This allows Equation (12) to rewritten as

$$h_0 + q + \frac{u_0^2}{2} = h_1 + \frac{u_1^2}{2} \tag{16}$$

while Equation (4) can be rearranged into

$$u_0^2 = v_0^2 \frac{(P_1 - P_0)}{v_0 - v_1} \tag{17}$$

$$u_1^2 = v_1^2 \frac{(P_1 - P_0)}{v_0 - v_1} \tag{18}$$

and combined to form the Hugoniot Curve

$$h_1 - (h_0 + q) = \frac{1}{2}(u_0^2 - u_1^2) = \frac{1}{2}(v_0 + v_1)(P_1 - P_0) \tag{19}$$

Assuming perfect gas so that the caloric equation of state for sensible enthalpy

$$h = \frac{\gamma}{\gamma - 1} Pv \tag{20}$$

can be introduced, where γ is the ratio of specific heats. This allows the Hugoniot curve

to be rearranged into

$$(\gamma + \alpha)(x - \alpha) = \beta \tag{21}$$

$$\alpha \equiv \frac{\gamma_1 - 1}{\gamma_1 + 1} \tag{22}$$

$$\beta \equiv \frac{\gamma_1 - 1}{\gamma_1 + 1}\left(\frac{\gamma_0 + 1}{\gamma_0 - 1} - \frac{\gamma_1 - 1}{\gamma_1 + 1} + \frac{2q}{P_0 v_0}\right) \tag{23}$$

or, in a more convoluted but more easily plotted form,

$$y = \frac{\frac{\gamma_0 + 1}{\gamma_0 - 1} - x + \frac{2q}{P_0 v_0}}{\frac{\gamma_1 + 1}{\gamma_1 - 1}x - 1} \tag{24}$$

which, when added to the plot with the Rayleigh Curve, results in Figure 11.
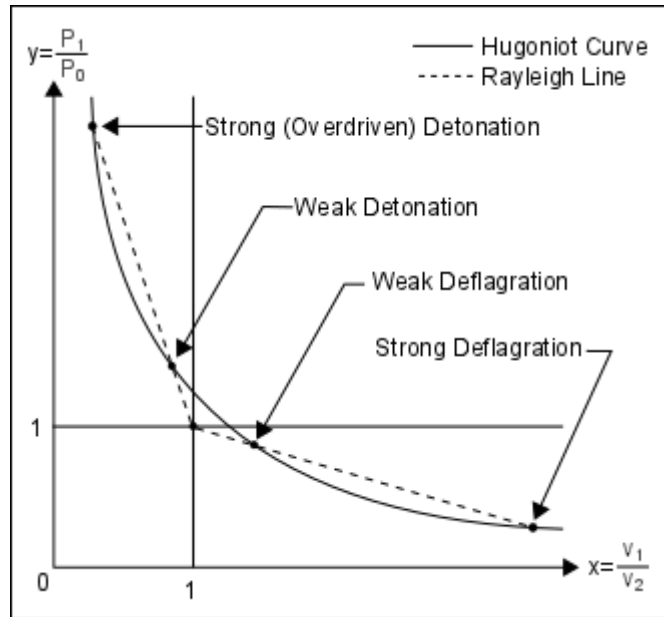
Figure 11. Rayleigh Line and Hugoniot Curve intersections on P-v ratio plane.

The locations where the Rayleigh Line and Hugoniot Curve intersect are points where the conservation of mass, momentum, and energy conservation equations are all satisfied. The Hugoniot Curve is a locus of downstream states for given upstream states. The reaction begins at (1,1), progressing along the Rayleigh Line as the reactants are converted into products, until it reaches the intersection point with the Hugoniot Curve, where it is assumed that the reaction is complete [13].

Chapman-Jouguet Criterion

The above process gives four distinct possibilities for the final state of the products once the reaction is complete: strong and weak detonations, and strong and weak

deflagrations. There are two more possibilities, the Chapman-Jouguet, or CJ solutions, in which the Rayleigh Line is tangent to the Hugoniot Curve, as shown in Figure 12.
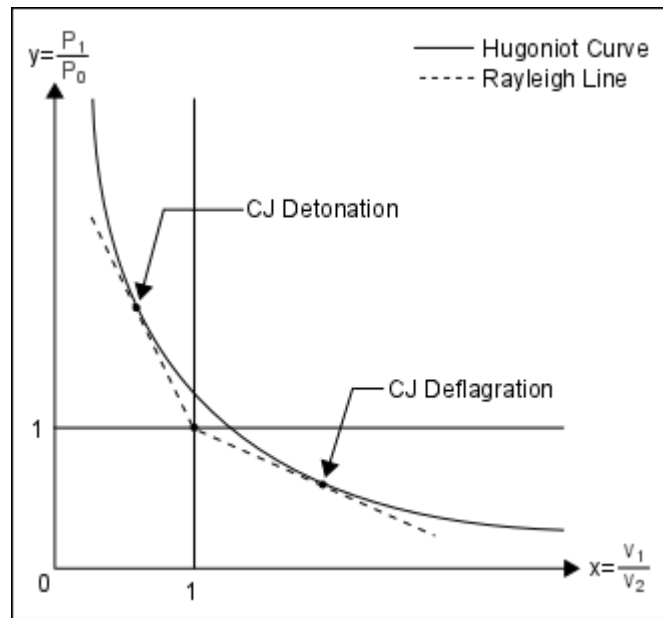
Figure 12. CJ (tangency) solutions to Rayleigh Line and Hugoniot Curve.

The upper CJ solution, for detonation, is important because it agrees remarkably well with experimentally observed combustion wave behavior. The lower CJ solution, for deflagration, is not as well replicated because the slower speed of the wave allows it to affect upstream conditions before arrival, and the wave itself is affected by boundary conditions downstream [13]. Because of the agreement of the upper solution with experiments, it is of value to calculate the flow velocity for these conditions. This requires first identifying the point itself, and then determining the velocity from some quality of the point.

To find the point, the slopes of the Rayleigh Line and Hugoniot Curves are set equal to one another. Because the goal of this calculation is to determine the velocity of the combustion wave, it is more convenient to rearrange the slope of the Rayleigh Line into

$$\left(\frac{dy}{dx}\right)_R = \frac{1-y}{1-x} \tag{25}$$

where subscript R refers to Rayleigh, and the slope of the Hugoniot Curve into

$$\left(\frac{dy}{dx}\right)_H = \frac{y+\alpha}{\alpha-x} \tag{26}$$

where subscript H refers to Hugoniot, before equating the two.

This results in the relationship

$$y^* = \frac{-x^*(1-\alpha)}{1+\alpha-2x^*} = \frac{-x^*}{\gamma_1-(\gamma_1+1)x^*} \tag{27}$$

where the superscript * refers to the CJ solutions. Inserting the latter value into the Rayleigh Line slope formula (25) allows the slope of the Rayleigh Line (and by extension, the Hugoniot Curve) at the CJ point to be written as

$$\left(\frac{dy}{dx}\right)_R^* = \left(\frac{dy}{dx}\right)_H^* = \left(\frac{dy}{dx}\right)^* = \frac{\gamma_1}{\gamma_1-(\gamma_1+1)x^*} \tag{28}$$

with the dependence on y removed. Multiplying the numerator and denominator of Equation (28) by x^* makes the equation take the form

$$\left(\frac{dy}{dx}\right)^* = \frac{\gamma_1 x^*}{(\gamma_1 - (\gamma_1 + 1)x^*)x^*} \tag{29}$$

which includes the components of Equation (27). Replacing those components with y^* allows Equation (29) to be simplified into the form

$$\left(\frac{dy}{dx}\right)^* = -\gamma_1 \frac{y^*}{x^*} \tag{30}$$

From Equations (27) and (30), the slope and location of the upper CJ point are established. Further relations are required to derive velocity information from these. Making the reasonable approximation that the flow of the products post-combustion is isentropic, they would be subject to the relation

$$P_1 v_1^{\gamma_1} = constant \tag{31}$$

which implies that

$$yx^{\gamma_1} = constant \tag{32}$$

Implicit differentiation shows that

$$\left(\frac{dy}{dx}\right)_s = -\gamma_1 \frac{y}{x} \tag{33}$$

where subscript s represents isentropic. This slope is the same as that of the Rayleigh Line and Hugoniot Curve, from Equation (30). This allows properties of the isentropic slope to

26

be equated to the other slope values to draw out velocity characteristics at the CJ points. Similar to Equation (31), the isentropic flow would be subject to

$$\frac{dP_1}{P_1} = \gamma_1 \frac{d\rho_1}{\rho_1} \tag{34}$$

which can be rearranged into

$$\frac{dP_1}{d\rho_1} = P_1 \gamma_1 v_1 = c_1^2 \tag{35}$$

This equation has useful velocity information, but it must be converted into dy/dx format to equate to the other slopes. One way to do this is

$$\left(\frac{dy}{dx}\right)_s = \frac{dP_1}{d\rho_1} * \frac{dy}{dP_1} * \left(\frac{dx}{dv_1}\right)^{-1} * \frac{d\rho_1}{dv_1} = \frac{-1}{P_0 v_0 x^2} \left(\frac{dP_1}{d\rho_1}\right) = \frac{-c_1^2}{P_0 v_0 x^2} \tag{36}$$

where $dP_1/d\rho_1$ can be found from Equation (35); dy/dP_1 is found from Equation (6); dx/dv_1 is found from Equation (7); and $d\rho_1/dv_1$ is from the definition of density and specific volume.

Combining Equations (18) and (25) produces the slope equation

$$\left(\frac{dy}{dx}\right)_R = \frac{-u_1^2}{P_0 v_0 x^2} \tag{37}$$

which can be equated to the slope of the isentrope to yield

27

$$\left(\frac{dy}{dx}\right)_R = \frac{-u_1^2}{P_0 v_0 x^2} = \left(\frac{dy}{dx}\right)_S = \frac{-c_1^2}{P_0 v_0 x^2} \tag{38}$$

Therefore

$$(M_1^*)^2 = \left(\frac{u_1^*}{c_1^*}\right)^2 = 1 \tag{39}$$

which would mean that the downstream gas leaves the combustion wave at a sonic condition. This relation was used by Jouguet to justify the importance of the CJ condition, along with the fact that it is the position on the Hugoniot curve which exhibits the minimum value of entropy change across the wave. Chapman justified the validity of the solution by the fact that it is the minimum velocity detonation condition that satisfies the conservation equations, along with the equation of state [13].

Of the three possible detonation states (strong, weak, and CJ) shown in Figure 11 and Figure 12, the strong solution is unstable for freely propagating combustion waves, as the subsonic flow behind it allows disturbances to reach and attenuate the wave [13]. The scenario can exist, but it requires a driving piston to support the reaction.

The weak detonation case is possible if multiple intersecting Hugoniot curves are constructed as a function of the reaction progress, and are referred to as pathological detonations. Figure 11 and Figure 12 indicate that the pressure ratios which they would exhibit would be lower than those from the CJ solutions, however, and so the conditions of weak detonation cases are less relevant to the design of the tube.

The above calculations are useful for establishing the characteristics of the detonation for which they should be designed, but they cannot be used to determine the velocity or pressure ratio of a detonation wave from initial and boundary conditions on their own. For that, it is necessary to introduce the Rankine-Hugoniot relations[13, 21].

Rankine-Hugoniot Relations

Whereas the previous calculations rely exclusively on an equation of state, the conservation of mass, momentum, and energy equations, and the experimentally supported (but not rigorously proven through theory) CJ criterion, the Rankine-Hugoniot relations allow the determination of downstream state properties as functions of initial and boundary conditions. Doing this requires the additional specification that the rate of chemical energy release is constant, and therefore independent of the downstream state [13, 21].

As the CJ points are the standard solutions to predict detonation wave behavior, the first goal is to determine $M_{CJ_{Det}}$, the Mach number of the detonation wave CJ solution, which is equal to the particle velocity of the reactants in a wave-fixed coordinate system. To begin, the "y" value of the Rayleigh Line, from Equation (11), and that of the Hugoniot Curve, from Equation (24), are set equal to one another. This yields the quadratic equation

$$x^2 - 2\frac{\gamma_1(\gamma_0 + \eta)}{\gamma_0(\gamma_0 + 1)}x + \frac{\gamma_1 - 1}{\gamma_1 + 1}\left[1 + 2\eta\left(\frac{1}{\gamma_0 - 1} + \frac{q}{\gamma_0 P_0 v_0}\right)\right] = 0 \qquad (40)$$

$$\eta \equiv \frac{1}{M_0^2} \tag{41}$$

the roots of Equation (40) can be solved via the quadratic formula

$$x = \frac{-b \pm \sqrt{b^2 - 4ac}}{2a} \tag{42}$$

which returns a pair of values for x of

$$x = \frac{v_1}{v_0} = \frac{\rho_0}{\rho_1} = \frac{\gamma_1(\gamma_0 + \eta \pm S)}{\gamma_0(\gamma_1 + 1)} \tag{43}$$

$$S \equiv \sqrt{\left(\frac{\gamma_0}{\gamma_1} - \eta\right)^2 - K\eta} \tag{44}$$

$$K \equiv \frac{2\gamma_0(\gamma_1 + 1)}{\gamma_1^2} \left[\frac{\gamma_1 - \gamma_0}{\gamma_0 - 1} + \gamma_0(\gamma_1 - 1)\frac{q}{\gamma_0 P_0 v_0}\right] \tag{45}$$

where S and K are defined to simplify notation. The $\pm S$ value in Equation (43) defines the difference between which solution is indicated on Figure 11, with a positive value corresponding to a weak detonation or strong deflagration and a negative value indicating a strong detonation or weak deflagration. The larger the value of S, the further apart the solutions are on the Hugoniot Curve, both from each other and from the CJ points, indicating that the Rayleigh Line is intersecting it at more distant locations. When the value of S is zero, the two solutions coincide and the indicated solution corresponds to the

CJ points, with M_0 becoming M_{CJ} in the process. Setting $S = 0$ and solving Equation (43) for η as an intermediate step towards determining M_{CJ} produces the relation

$$\eta^* = \frac{1}{M_{CJ}^2} = \frac{\gamma_0}{\gamma_1}\left(1 - \frac{2}{1 \pm \sqrt{1 + \frac{4}{K}\frac{\gamma_0}{\gamma_1}}}\right) \tag{46}$$

where the $\pm$ quantity designates whether the value pertains to a CJ detonation (positive) or CJ deflagration (negative). The value "$q/\gamma_0 P_0 v_0$" in Equation (45) has a magnitude of approximately 30 for real detonatable mixtures, which means that the value of $1/K$ in Equation (46) is less than one, and the square root quantity can be approximated by a binomial series expansion[13]. In this case the approximation is

$$\sqrt{1 + \frac{4}{K}\frac{\gamma_0}{\gamma_1}} \approx 1 + \frac{1}{2}4\left(\frac{\gamma_0}{\gamma_1}\right)\frac{1}{K} + O\left(\frac{1}{K^2}\right) \approx 1 + \frac{2}{K}\left(\frac{\gamma_0}{\gamma_1}\right) \tag{47}$$

where the terms of order $1/K^2$ and above are neglected because they will have a magnitude much smaller than one. Replacing the square root value in Equation (46) with the approximation and choosing the positive root for CJ detonation values produces

$$\eta^* = \frac{1}{M_{CJ_{Det}}^2} \approx \frac{\gamma_0}{\gamma_1}\left(1 - \frac{2}{1 + 1 + \frac{2}{K}\left(\frac{\gamma_0}{\gamma_1}\right)}\right) \approx \left(\frac{\gamma_0}{\gamma_1}\right)^2\frac{1}{K} \tag{48}$$

which can be solved for $M_{CJ_{Det}}$, the Mach number of the wave for the CJ detonation solution, in terms of K. Assuming that $\gamma_0 \approx \gamma_1$, K from Equation (45) simplifies to

31

$$K \approx 2(\gamma_1^2 - 1)\frac{q}{\gamma_0 P_0 v_0} \tag{49}$$

When Equation (48) is solved for $M_{CJ_{Det}}$, the value simplifies to

$$M_{CJ_{Det}} \approx \frac{1}{\sqrt{\eta^*}} \approx \sqrt{2(\gamma_1^2 - 1)\frac{q}{\gamma_0 P_0 v_0}} \tag{50}$$

This value can be used in the Rankine-Hugoniot relationships, which are dependent on the Mach number of the combustion wave, but do not require the above approximations to derive. The first is the ratio of the product and reactant densities, and it is found by inverting the value of x from Equation (43) to find

$$\frac{\rho_1}{\rho_0} = \frac{1}{x} = \frac{\gamma_0(\gamma_1 + 1)}{\gamma_1(\gamma_0 + \eta \pm S)} \tag{51}$$

The ratio of flow velocities can be determined from the conservation of mass Equation (1)

$$\frac{u_1}{u_0} = \frac{\gamma_1(\gamma_0 + \eta \pm S)}{\gamma_0(\gamma_1 + 1)} \tag{52}$$

The pressure ratio can be determined using the conservation of momentum Equation (2)

$$\frac{P_1}{P_0} = \frac{\gamma_0 + \eta \pm \gamma_1 S}{(\gamma_1 + 1)\eta} \tag{53}$$

The induced product velocity ratio in laboratory-fixed coordinates can be determined from the conservation of mass and the coordinate transformation shown in Figure 8

$$\frac{u_1{}'}{u_0} = \frac{\gamma_0 - \gamma_1(\eta \pm S)}{\gamma_0(\gamma_1 + 1)} \tag{54}$$

Finally, the product pressure is often normalized by the quantity $\rho_0 D^2$ as in

$$\frac{P_1}{\rho_0 D^2} = \frac{\gamma_0 + \eta \mp \gamma_1 S}{\gamma_0(\gamma_1 + 1)} \tag{55}$$

These five Equations, (51)-(55), constitute the Rankine-Hugoniot relationships. They can be used to predict the behavior of a detonation wave based on initial conditions, and they are easily estimated for the CJ detonation condition by using the value of η from Equation (46) or the even simpler estimate from Equation (50) and Equations (44) and (45) for S and K, respectively.

Their use is not limited to the CJ conditions, however. If S is not assumed to be zero and η is found from Equation (41), using another method to determine the Mach number of the combustion wave, they can predict the strong and weak detonation and deflagration conditions as well, although these solutions are not as accurate because they do not consider the wave structure.

The main limitation of the criterion discussed is that they are insufficient to calculate whether or not a detonation will occur given a set of conditions. The user must decide whether a combustion wave will be generated and whether it will be a detonation or deflagration wave through other means.

Detonation Structure

ZND Model

The previous analysis ignored the structure of the wave in question, i.e. what happens within the wave itself, but it is important to have a general idea of the process that the gas goes through during its transformation. The simplest form that this can take for detonations is a steady, laminar, one-dimensional structure, the standard version of which is the Zeldovich-Von Neumann-Döring, or ZND, model. Actual detonation waves are inherently unstable, but the ZND model can be a useful tool for analysis and conceptualization, especially with regards to characteristic length scales and reaction kinetics. The basic layout of the ZND structure is shown in Figure 13.
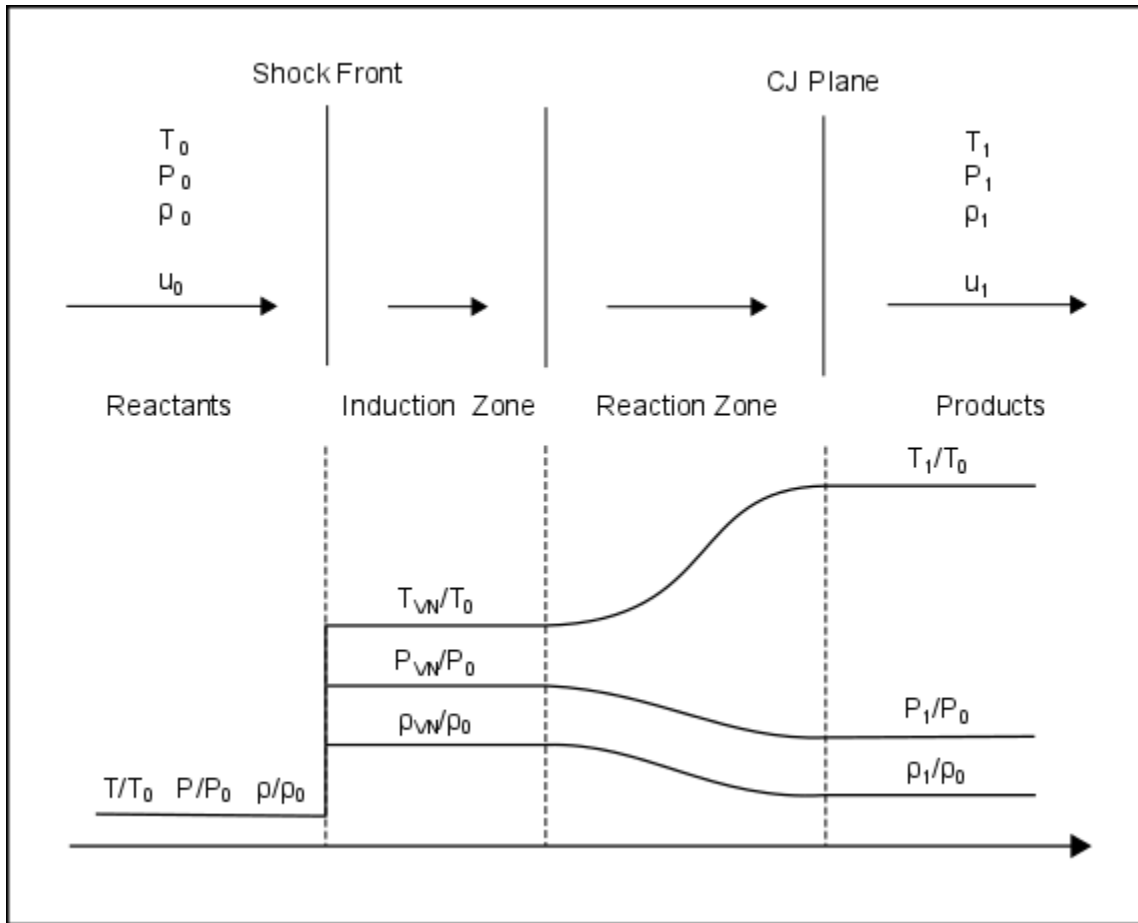
Figure 13. Schematic and characteristics of ZND structure regions.

The reactants enter the shock front, which adiabatically raises the temperature, pressure, and density of the medium. These remain nearly constant as they pass through the induction zone, as radicals are generated from the high-temperature condition. Rapid reactions take place in the reaction zone, causing the gas to expand and lose pressure and release further heat. For unsupported detonations, the gas eventually expands further, accelerating away from the wave and driving the wave forward, although this is not shown

in Figure 13. The subscript VN represents the "Von Neumann State" immediately following the shock, which can be calculated using the normal shock relations.

It is possible to calculate an expected length for the ZND reaction zone for inviscid, perfect gasses using conservation equations and a reaction rate relation. First, the VN state is calculated, then the kinetic rate equation is integrated for the elementary reactions along the Rayleigh line. This is important as it yields a characteristic length for the fundamental chemical processes taking place within the combustion wave.

The CJ solutions and results of the ZND model agree remarkably well with experimental results, which is somewhat surprising given the fact that the structure does not represent real detonations. The overwhelming majority of real world versions are inherently unstable, transient, and three-dimensional. Many types are possible, but as the detonation tube is cylindrical in nature, the discussion will be restricted to the two main cylindrical types, spinning and cellular detonations.

Spinning Detonations

While spinning detonations are 3D transient relative to a laboratory plane, they are steady when considering a reference frame spinning with the detonation head. The wave front curves and creates a fold where the slope of the shock front changes abruptly. This fold extends to the wall, causing a localized region of intense reaction which rotates around the circumference of the confinement. This is because the fold must keep up with the axial velocity of the detonation head and also propagate around the exterior of the tube, requiring a higher velocity than the rest of the detonation front and producing a suitably

more significant pressure and temperature increase through the normal shock relations. Shchelkin modeled this as shown in Figure 14.
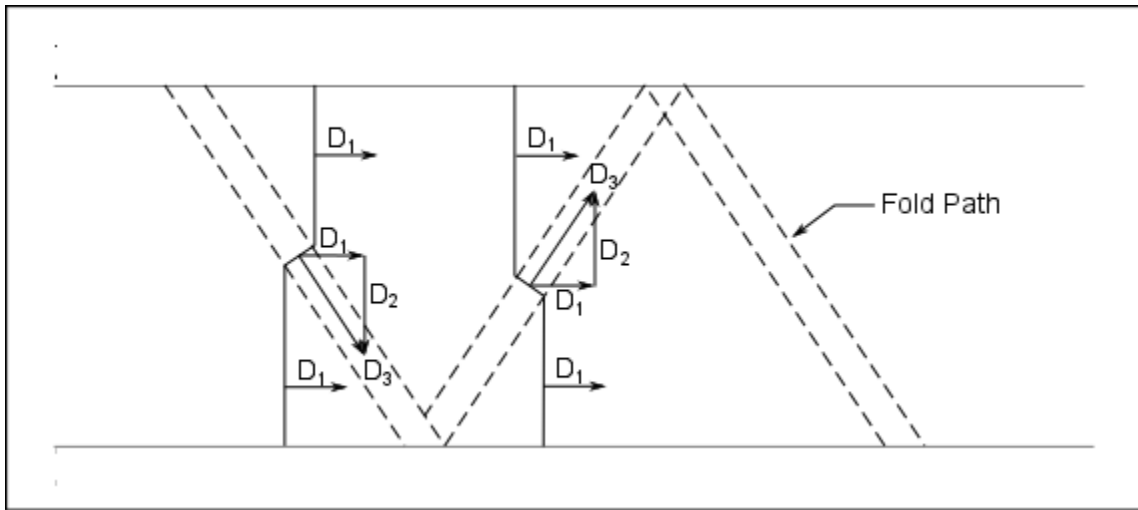

Figure 14. Shchelkin model showing fold path for spinning detonation front.

Here the subscripts 1, 2, and 3 do not represent products and reactants, but different velocities of the shock front depending on the location on the detonation head. From the figure it is noticeable that the velocity of the front in the fold, D_3, surpasses that of the rest of the head, D_1, which is close to the CJ velocity. However, only one fold is drawn. Some spinning detonations have multiple folds, and are referred to as multiheaded detonations. The folds can rotate in tandem or opposite directions.

Cellular Detonations

Spinning detonations are more likely to occur near the limits at which detonations can be sustained. Detonation waves are inherently unstable, and though spinning detonations and other particular propagation cases exist, cellular detonations can exist over a broader spectrum of conditions [13, 22]. The "cells" are locations where the detonation front expands out in multiple locations, and sometimes look like a net has been tightened on a balloon. The "creases" that form the cells require transverse rather than axial shock waves to exist, and so the position and size of the cells can change constantly, hence the unstable descriptor. The structure of the cells formed by the intersections of the transverse waves and detonation front is referred to as the substructure.

Due to the cells, the detonation velocity can vary within the substructure from 0.6 to 1.8 times the CJ detonation velocity, although the time average will still equal that of the CJ solution. The structure of the wave is heavily influenced by the boundary conditions of the tube.

Various mixtures have distinct characteristic cell sizes, which are often measured experimentally with smokefoils, sheets of metal covered with a layer of soot from kerosene burned inefficiently in air. When the fold of a spinning detonation or the boundary of a detonation cell passes by this device, the locations of intersecting shock slopes removes more soot than the main body of the wave, leaving distinct patterns on the sheet which can be used to draw conclusions about the substructure of the wave. The smokefoils can be placed on the tube sidewalls or endwall, though the additional analysis length provided by the sidewall method is known to achieve more accurate measurements.

38

The smokefoil patterns generated by spinning detonations are reminiscent of the pattern shown in Figure 14, with more cuts added for additional heads, and those created by cellular detonations are shown in Figure 15.
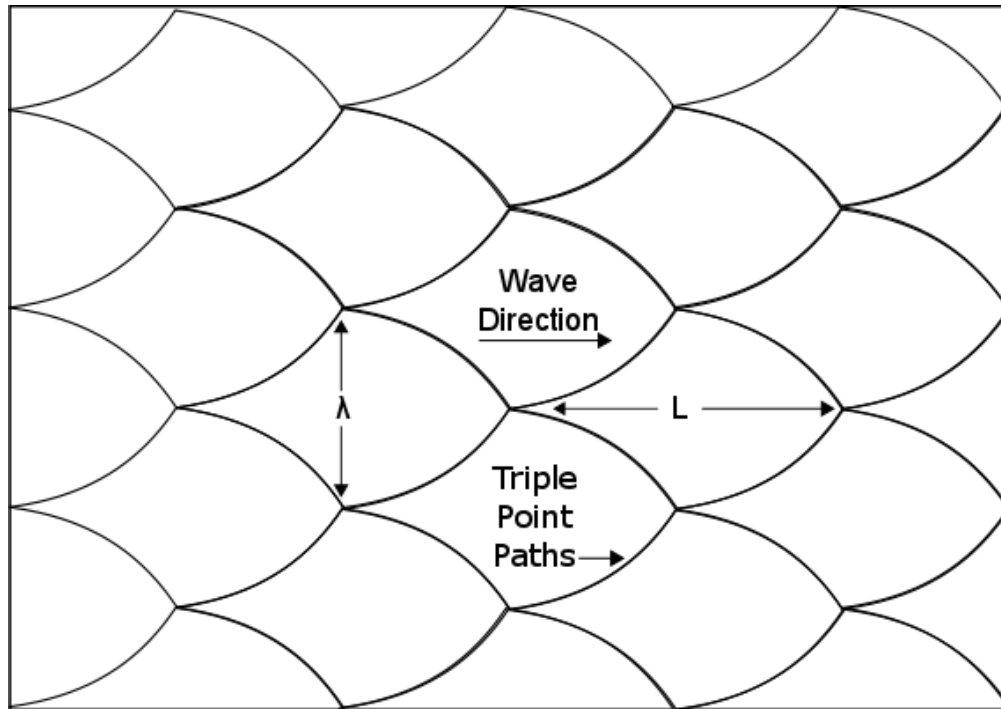

Figure 15. Patterns shown on sidewall smokefoil from cellular detonation [13].

The two characteristic lengths that can be determined from smokefoils, λ and L, are the cell size and length, respectively. The cell size can also be estimated from the ZND reaction zone length calculation and an experimental data point, as a simple linear relationship between cell size and reaction zone length was found to have a reasonable accuracy [23]. The relationship is

$$\lambda = Al \tag{56}$$

where A is a constant determined from the data point, and l is the reaction zone length as calculated for the ZND structure.

Deflagration-to-Detonation Transition (DDT)

Unless directly initiated by a large, sudden energy input, detonation waves begin as deflagration waves, which accelerate to a critical velocity before transitioning. This process can be significantly affected by obstacles, which cause the flame front to wrap around them, increasing the surface area of the wave front. Because deflagrations are dominated by diffusion, this can cause the flame to accelerate until it reaches a suitable velocity to transition into a detonation wave [24]. Wall roughness can contribute to this as well.

In smooth tubes, the deflagration wave will accelerate until it reaches a velocity approximately half that of the CJ detonation velocity before transitioning, spiking to a supersonic (overdriven) velocity before finally decaying to the CJ condition. The actual onset of the detonation has multiple potential causes; precursor shock waves can merge, hot spots in the reaction zone can become explosion centers, developing blast waves that merge with the precursor shock, or a retonation wave could form as part of the precursor shock reflects back into the combustion products [13, 22].

Two parameters that are characteristic to the DDT process are blockage ratio and run-up length. The blockage ratio is defined as

$$BR = 1 - \left(\frac{d}{D_i}\right)^2 \tag{57}$$

where BR is the blockage ratio, d is the orifice diameter allowed by the blockages, and D is the internal tube diameter [13]. The run-up length is the distance required from ignition source to transition to detonation, and can be measured by pressure transducers or photodiodes placed along the length of the tube, which will register a sudden velocity change in the wave. As it depends on initial conditions, boundary conditions, and chemical composition, estimation from elementary parameters has not been successful [13]. Numerical simulations have been created to predict the process, but because of the wide variety of possible input parameters, validation and experimentation will be vital for the foreseeable future [25, 26].

Describing the effects of the various possible boundary conditions is far outside the scope of this work, as a great number of possibilities exist. Suffice it to say that they are significant, and do not even need to protrude significantly into the free path of the wave. Rough walls alone can allow detonations to propagate significantly below the CJ velocity (about 30%) [13].

Detonation Limits

Whether or not a detonation can occur is not determined solely by the ability of the deflagration wave to accelerate, but also by the concentration of fuel and oxidizer in the mixture, the initial conditions of the mixture, and the boundary conditions of the enclosure, including the roughness, quality and geometry. As most experiments are

41

performed in rigid cylindrical tubes, the boundary conditions are usually specified and then the composition limits are determined experimentally [15, 27, 28].

As most detonations are cellular in nature, the primary focus of limits research corresponds to this type of event. Far from the limits, the cell size is small relative to the size of the enclosure, but near the limits the sizes are comparable.

Direct Initiation

As previously mentioned, initiating a detonation without the run-up distance requires a significant energy input to be delivered to the reactant mixture over a short time interval. This can be done in multiple ways, such as by introducing a suitably strong normal shock from an inert mixture, the detonation of an explosive charge, or even by photodissociation via pulses of ultraviolet light. A detonation could also be initiated in one part of a tube separated from the test region by a diaphragm, as these tend to cancel the detonation from the first section so that only a shock wave is introduced [13].

The strong blast wave generated from the source that directly initiates the detonation wave is overdriven, but quickly decays until it reaches the CJ condition. The minimum energy that must be provided at a point to initiate detonation can be calculated for a given mixture and initial conditions, but it requires preexisting data from the tube in order to determine the induction time.

4. FACILITY DESIGN AND PROCEDURE

Facility Overview

The proposed detonation tube facility would consist of the tube itself; the supports which hold it steady; a circulation system to facilitate faster mixing of the detonable mixture before testing; an inlet system to provide the initial gas mixtures; the redirection system that would deal with the high velocity exhaust from the open end of the tube; two inspection sections which could be removed from the tube to service the interior, modify internal mechanisms, or enable direct initiation via shockwaves; and the diagnostic systems used to measure pressure, radical emission, detonation cell characteristics and the structure of the reaction zone.

The tube details, as designed, would have an internal diameter of 70 cm, a wall thickness of 12.7 mm, and an internal length of 100 m. Figure 16 shows a schematic of the design with several important components identified, and Figure 17 shows an isometric view of the tube model.
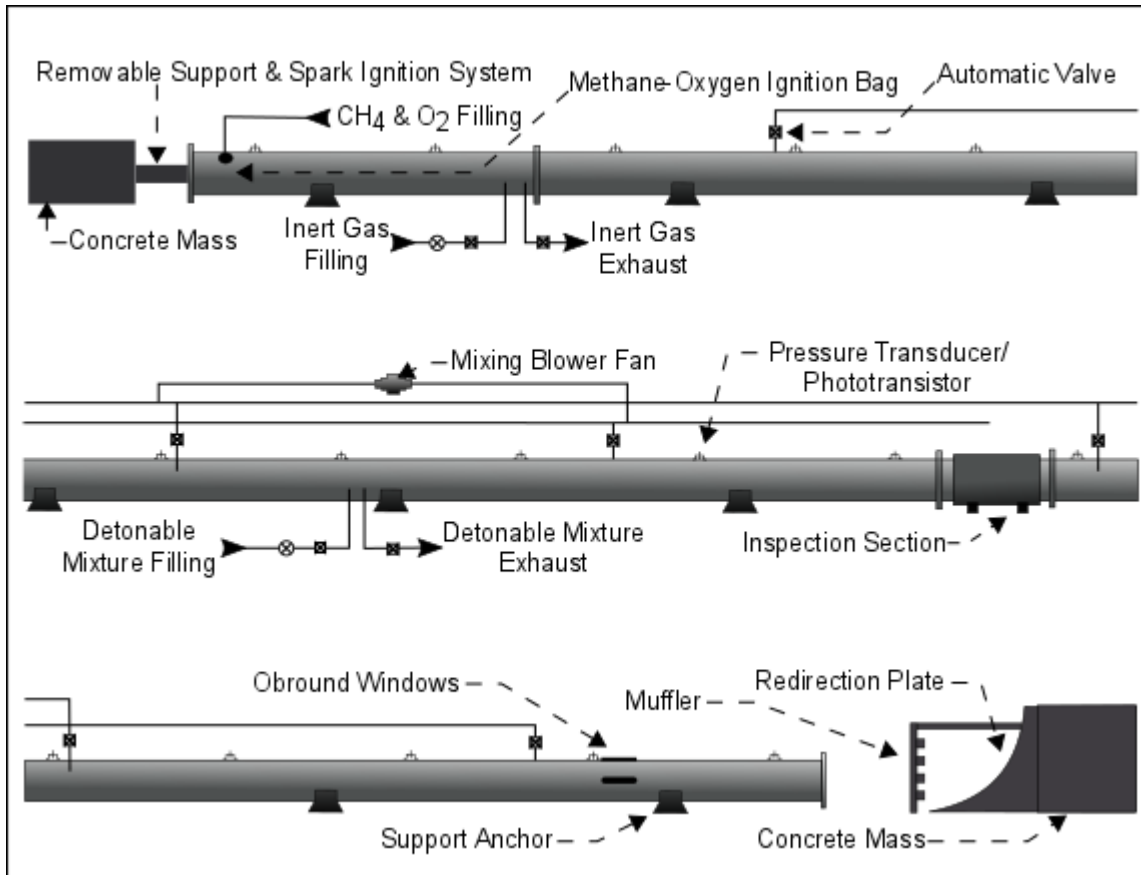
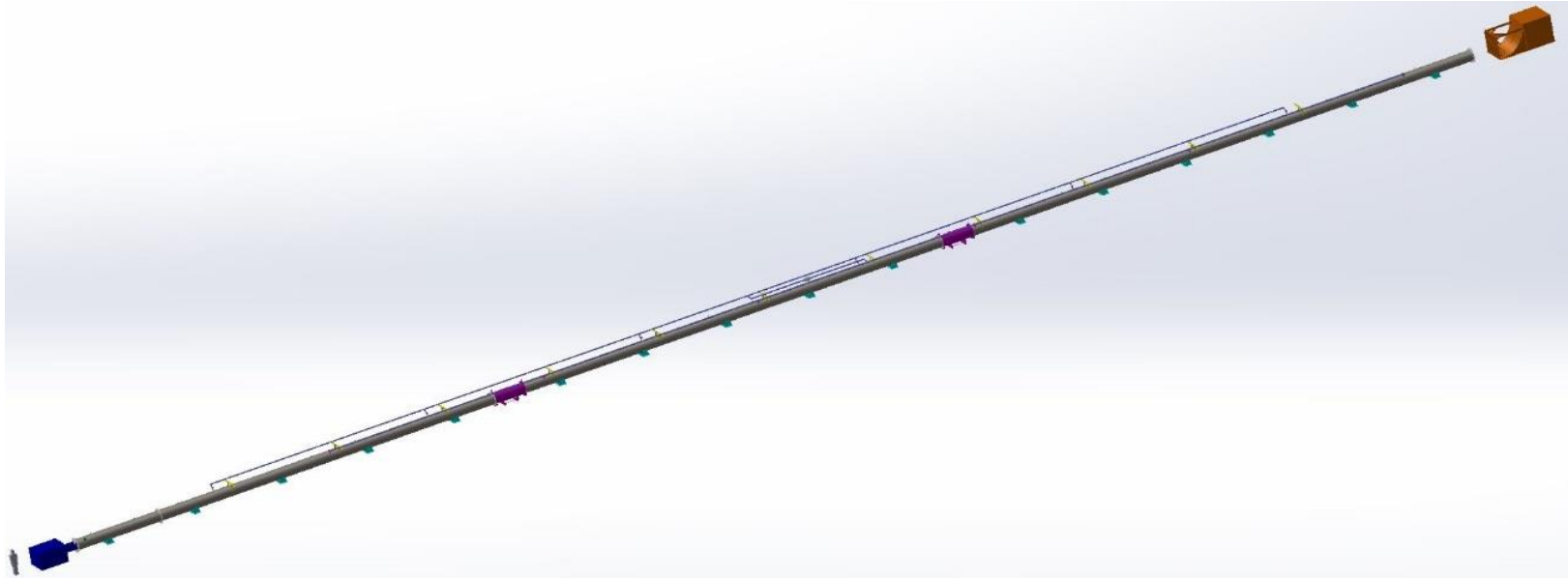**Figure 16. Schematic of detonation tube parts and piping diagram.**

Figure 17. Model of entire detonation tube from isometric perspective.

In order to present a better sense of scale, Figure 18 shows the tube model with the human model located at the right hand side of the tube. The same can be seen at the far left side of the full model in Figure 17.
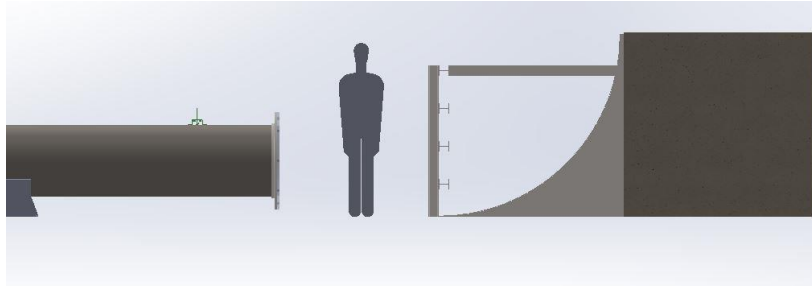

Figure 18. Model of end of detonation tube in profile with human model for scale.

Tube Body

The body of the tube would be constructed of industrial pipe commonly used by the oil industry in order to reduce initial costs and to take advantage of the manufacturing facilities in nearby Houston. The tubes would be welded end-on-end to each other and around the perimeter of the contact area with the support anchors. The tube would be closed on one end by a metal plate, and on the other by a plastic diaphragm clamped between two O-rings, designed to burst easily once the combustion wave reaches it.

The internal diameter of the tube would be 70 cm, and the overall length 100 m. The minimum required thickness was evaluated through two primary methods: 1) trends determined by experimentation with the GETF, and 2) hand calculation via the American

Society of Mechanical Engineers (ASME) Boiler and Pressure Vessel Code (BPVC) Section VIII Division I, which covers pressure vessels built in the United States.

The first thickness requirement comes from the experiences gathered at the GETF. They calculated a CJ pressure of 1.66 MPa, and numerical simulations showed the possibility of spikes of as much as 4.4 MPa due to shock reflections at localized pockets on the wall, lasting for very short durations. Spikes as high as 7 MPa were recorded during the life of the facility, likely occurring over very small areas. Due to the small size and duration of the predicted spikes, however, they decided on a thickness of 9.5 mm, which provided a factor of safety of 2.7. Throughout the use of the facility, no signs of deformation were observed, leading to a recommendation that the required tube thickness should follow the trend of

$$t = 9.5 * D_i \tag{58}$$

where t is the minimum thickness of a detonation tube. This translates to a required thickness of 6.65 mm for the proposed facility [7].

The second requirement to be satisfied used stress equations from the ASME. As this tube design would be used for similar gas mixtures as the GETF, it is reasonable to use their pressure estimates. Assuming a safety factor of 4 (the average factor of safety used for pressure vessels) from yielding, an internal pressure of 1.66 MPa, and ordinary ASTM A36 structural steel with a yield strength of 250 MPa, the minimum allowable thickness is 9.4 mm. From these two criteria, the chosen 12.7-mm thickness is allowable.

Support System

The support system is composed of the anchors that attach the tube to the foundation, the foundation itself, and the mass that resists the thrust caused by the action/reaction force developed as high-velocity gas exits the tube.

The tube will require a concrete pad to be laid beneath it, at least five feet wide and running the full length of the tube, plus extra distance to accommodate the heavy concrete blocks which will resist the thrust on each end.

The anchors are pipe saddles designed by Pipingtech, designed for large-diameter tubes. They will be bolted to the concrete to provide thrust resistance. Figure 19 shows the saddle geometry; because an exact size for the select tube was not found, a spacer will be employed.
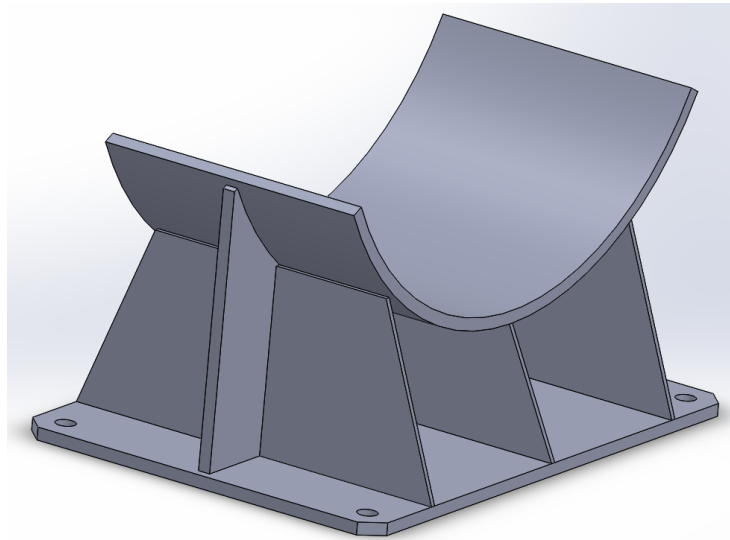

Figure 19. Tube support saddle made from welded plates.

The second component of the support system is the I-beam reinforcement connecting the end plate of the tube to a sizeable concrete support block, which is a part of the same concrete foundation underneath the tube. This is necessary as the detonation will tend to push against this plate as it is open at the far end. The block and I-beams are shown freestanding in Figure 20 and are connected to the tube in Figure 21.
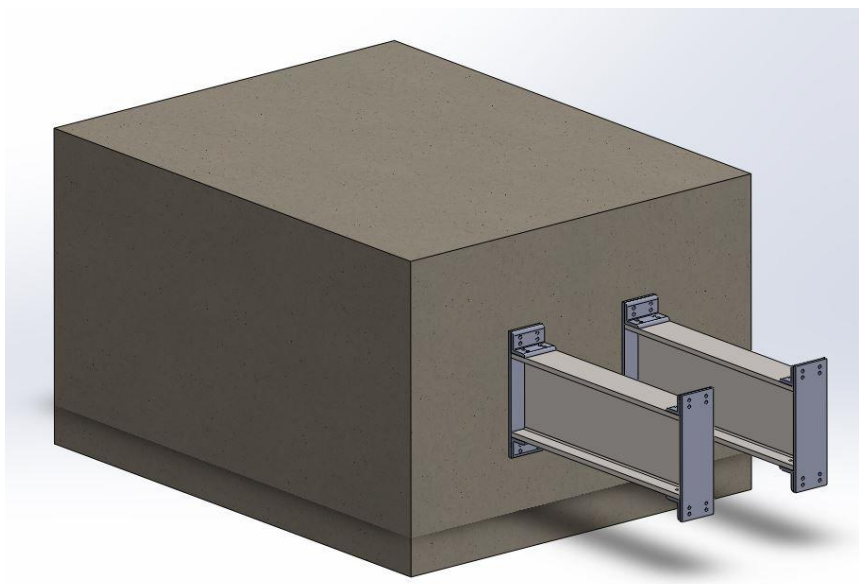

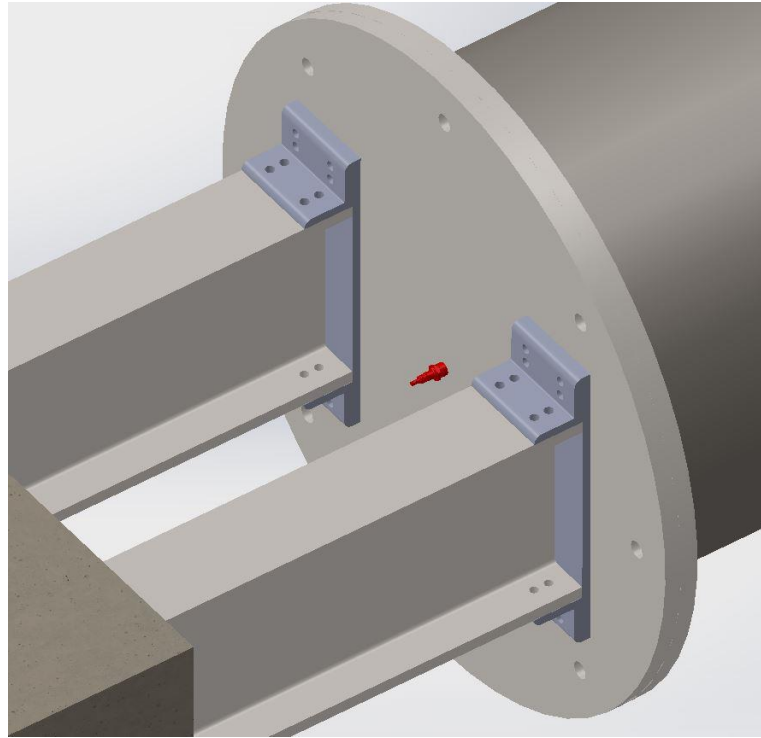**Figure 20. Concrete block and I-beam reinforcement for tube front.**

Figure 21. Tube front reinforcement attached to buildup plates on tube end, as well as spark ignitor.

The first tube segment is connected to the rest via a bolted flange, and the frontal support structure is removable to allow access or replacement of the first section of tubing. As this section contains the ignition systems and a variety of unique components, it is a likelier candidate for future upgrades than most of the rest of the build, and so it was designed to be modular.

Sealing Systems

Sealing must be achieved between removable sections of tubing (the inspection sections), for windows, and for the diaphragm which will seal off the end of the tube.

Between sections of tubing, O-rings in concentric grooves will be pressed against flat steel faces. Diaphragms will be sealed between two O-rings in grooves on metal faces, and when a diaphragm is not in use, these faces must accommodate a metal "dummy" ring which will compress the o-rings as a stand-in.

Filling System

Filling is controlled remotely from a reinforced room near the test facility through four distinct measurement systems depending on the degree of fidelity required. Initial filling will be measured with the help of flow meters; analogue pressure gages will enable rough control of concentrations; fine control will be achieved through use of pressure transducers; and capacitance manometers will regulate for the final fine-tuning. Figure 16 indicates filling locations; manual valves and manifolds located a distance away from the tube are excluded.

Mixing System

The mixing system needs to be able to circulate the reacting mixture quickly and thoroughly, should be cut off from the tube during the actual detonation process, and must be separable from the part of the tube located before the first inspection assembly in the event that a shock ignition is desired. The system consists of the manifold that distributes the gas, the supports which suspend it above the main tube, the valves which allow distribution to be controlled, and the blower which circulates the gas.

51

The manifold consists of smaller tubes on either side of the main tube, which connect to it via angled tubes. The inlet side and outlet sides alternate connections to the main tube to lessen the prevalence of gas drawing returning to locations nearby where it started. A simplified diagram of the mixing system can be seen in Figure 22, with the main tube in grey, the mixing system tubes in blue, automatic valves in red, and the main blower in green.
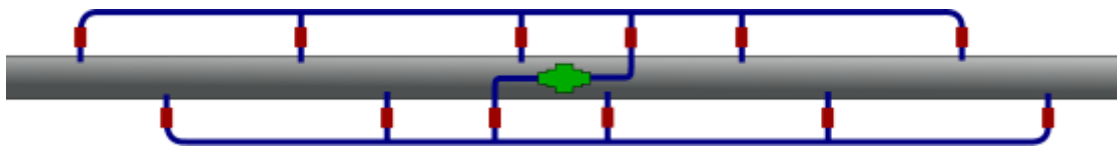

Figure 22. Diagram of mixing system attachment scheme.

Distribution is accomplished via automatic valves, as no personnel will be allowed within proximity of the tube while it is filled with detonable mixtures. The mixing manifold (blue) can be isolated from the tube body with automatic valves (red) at each connection point as in Figure 23. If fractionally controllable, these valves can be used to reduce the flow through the points nearest the blower, optimizing the circulation process.
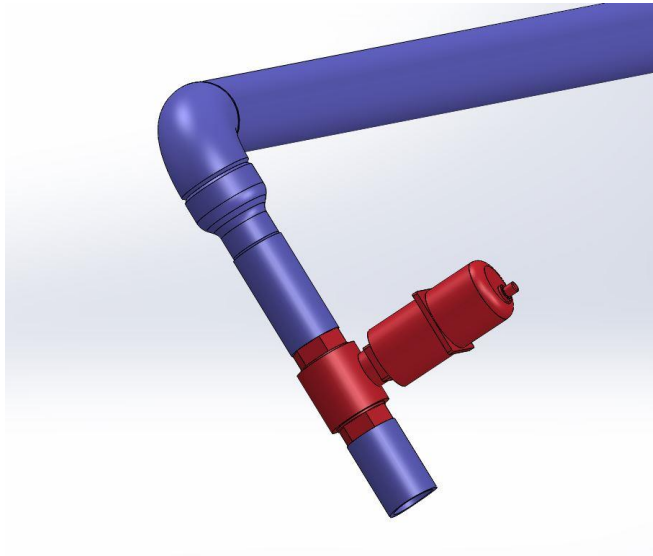
Figure 23. Automatic valve used in mixing system piping manifold.

The supports which suspend the manifold are constructed from welded I-beams as shown in Figure 24. Rounded sections are made via laser cutting to create a shape that can be welded to the tube body.

Figure 24. Tube support for mixing system piping manifold.

The main blower can be seen in green in Figure 25. To discourage circulation from only occurring between the connection points nearest the blower, it is attached to the manifold at a distance.
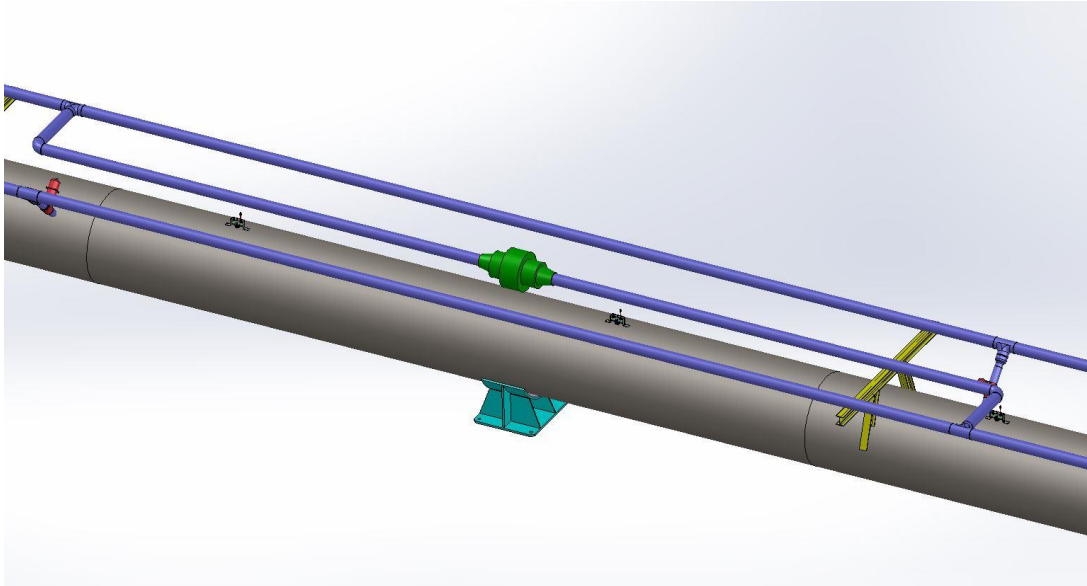

Figure 25. Main blower model for mixing manifold and piping attachment points.

Inspection Assembly

The inspection assembly has three main functions: first, it allows for the interior of the tube (and anything connected to it) to be examined for wear. Second, it enables improved ease of modification in event that obstructions or new devices need to be installed inside of the tube, and third, it can be used to enable direct initiation of detonations by clamping a diaphragm between two sections of the tube. Figure 26 shows the inspection assembly.
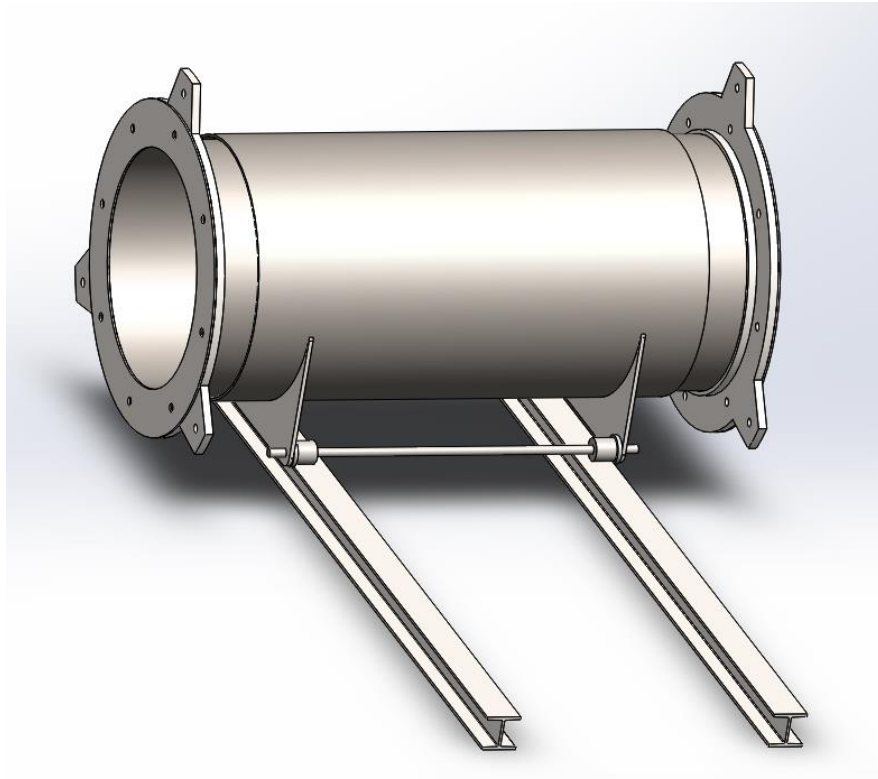
Figure 26. Model of inspection assembly in collapsed position.

It consists of a large diameter tube which acts as a sleeve covering two smaller internal-diameter tubes. Each of these has two O-ring grooves on their exterior diameters, which compress against the internal surface of the larger tube to seal. Two grooves are used instead of one to reduce the chance of angular misalignment between the small and large tubes, which could cause the edge of the small tube to grind against the interior of the larger. The O-rings enable the inner tubes to slide in and out so that they can either seal against an opposing surface or retract far enough to allow the inspection assembly to

be rolled away from the rest of the tube for alteration work to be done. The components in the inspection assembly are seen expanded in Figure 27.
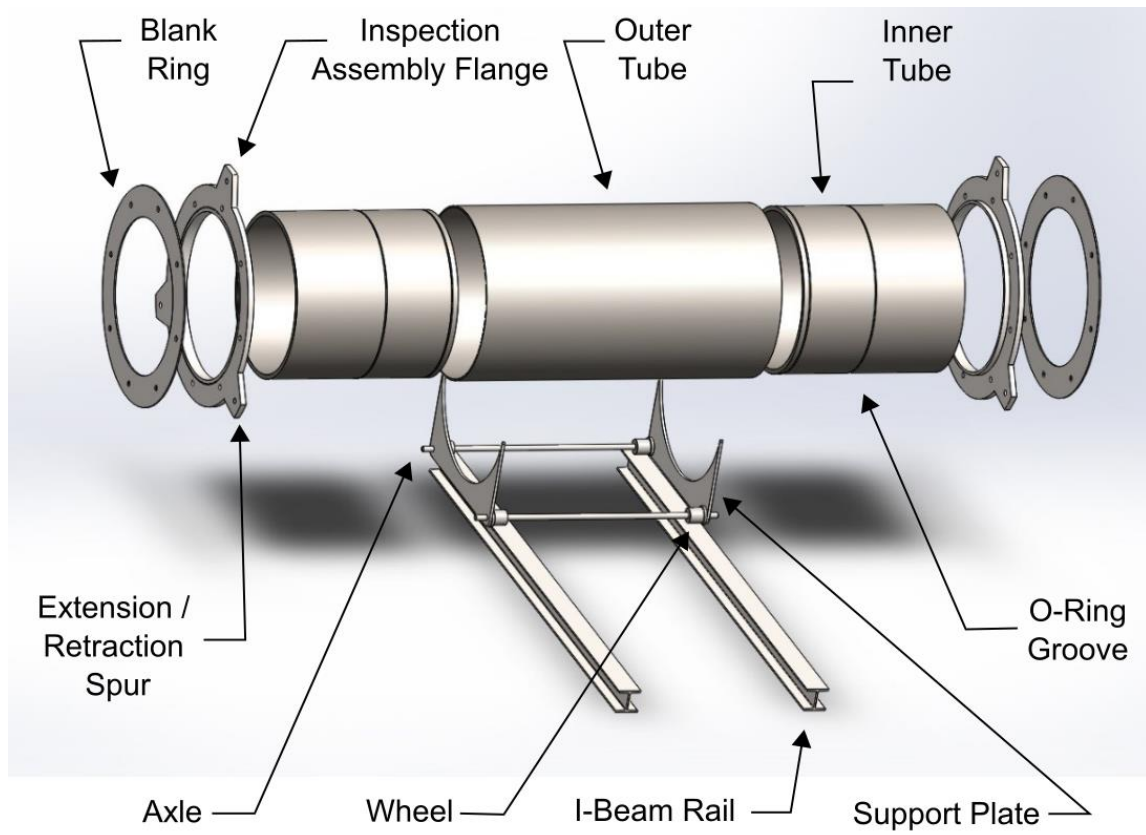

Figure 27. Expanded view of inspection assembly components.

When retracted, the inspection assembly appears as seen in Figure 28, which is color-coded to show the different components. The surrounding large tube is blue, inner retractable tubes are green, flanges are red, supporting plates which connect to the axles are orange, the axles themselves are red, the I-beam rails which they travel on are blue, and the yellow rings seen on the outside of the flanges are "blank rings". These have the

same internal diameter and bolt pattern as the main tube, and exist to compress the O-rings on opposing flanges when no diaphragm is being used. The ability to correctly compress and retain a diaphragm requires there to be two opposing O-ring grooves of the same diameter in adjacent flanges; these cannot seal against one another, so the blank rings are provided to supply the necessary sealing faces.
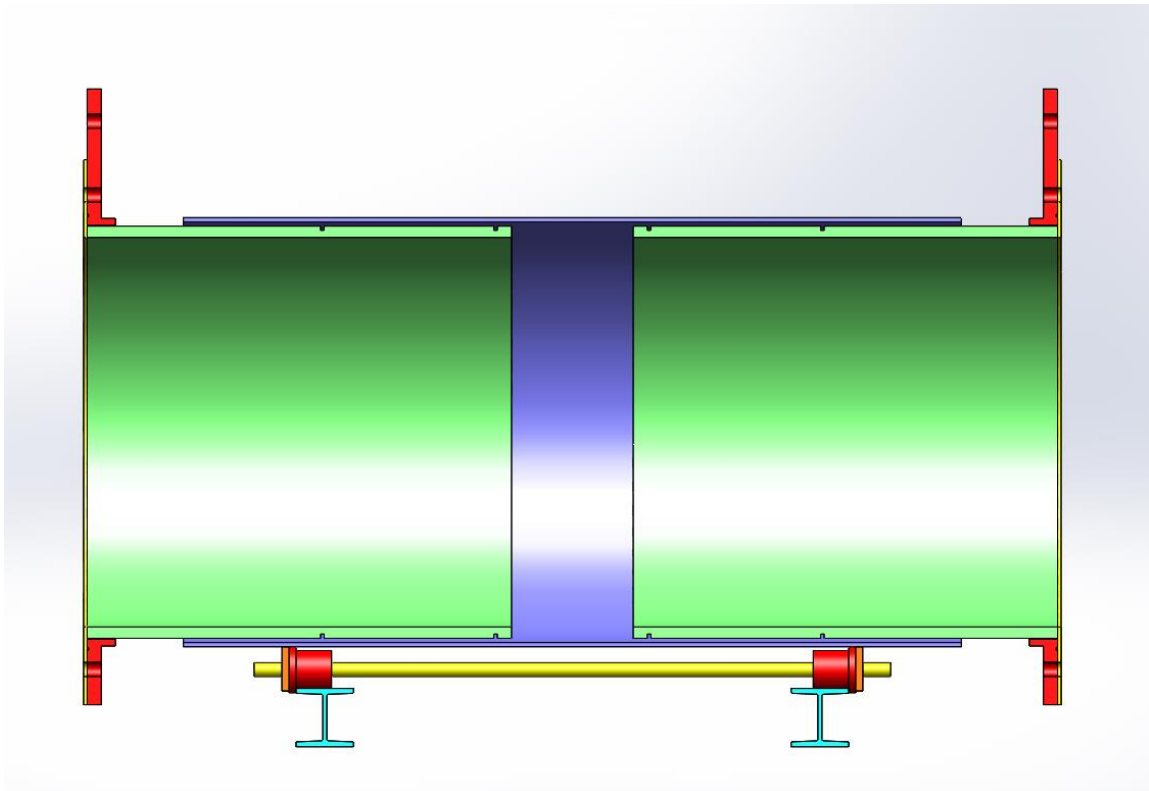

Figure 28. Section view of retracted inspection section, colored to show parts.

Two inspection assemblies would be included in the build, dividing the overall length roughly into thirds. Each inspection flange has three "extension/retraction spurs"

projecting from the outer diameter of the circular section, with bolt through-holes of the same diameter as the main bolts. These exist to allow easy extension and retraction of the inner tubes, should they prove to be too difficult to move by hand. A rod, thin enough to pass through the holes and having threaded sections on each end would be inserted through the holes on these spurs, and hex nuts on the inside or outside would allow significant force to be applied in order to extend or retract them.

Primary Ignition System

The primary ignition system allows for ignition via a spark plug, controlled by induction coils, located at the tube endwall; it can be seen colored red in Figure 21. This is the primary ignition source if the goal is to initiate a deflagration wave and observe the deflagration-to-detonation transition, both due to its location and due to the fact that it contributes the least amount of initial energy, making it unlikely to overtly affect the combustion process beyond initiation[29].

Explosive Bag Ignition System

The second method of ignition can be used for a more-energetic ignition or direct initiation of a detonation wave, depending on the application. It is initially triggered by a spark plug, as with the primary ignition system, but differs in that the spark plug is located inside a bag filled with a stoichiometric combination of methane and oxygen. This results in a rapid release of energy, and a force which can directly initiate detonation if the mixture is provided in a sufficient quantity. For the GETF, this meant a cylindrical bag filling the

internal diameter of the tube, one meter, for a length of three meters [19]. Figure 29 shows

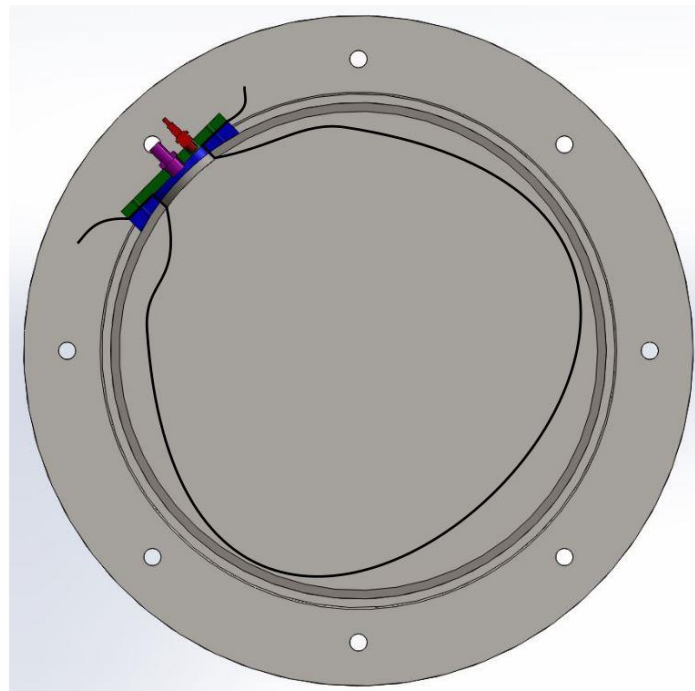a sketch of the bag placed into a sectioned view of the tube model.

Figure 29. Sketch of ignition system explosive bag.

The system consists of the bag, which is sealed by an O-ring between the tube-side

plate (blue) and free plate (green), which is threaded to accommodate the filling port

(purple) and the spark plug (red). The tube-side plate is machined to fit the cylindrical

profile of outside surface of the tube, to which it is welded. The O-ring runs in a groove

machined into its surface, which presses the bag against the free plate as it is bolted onto

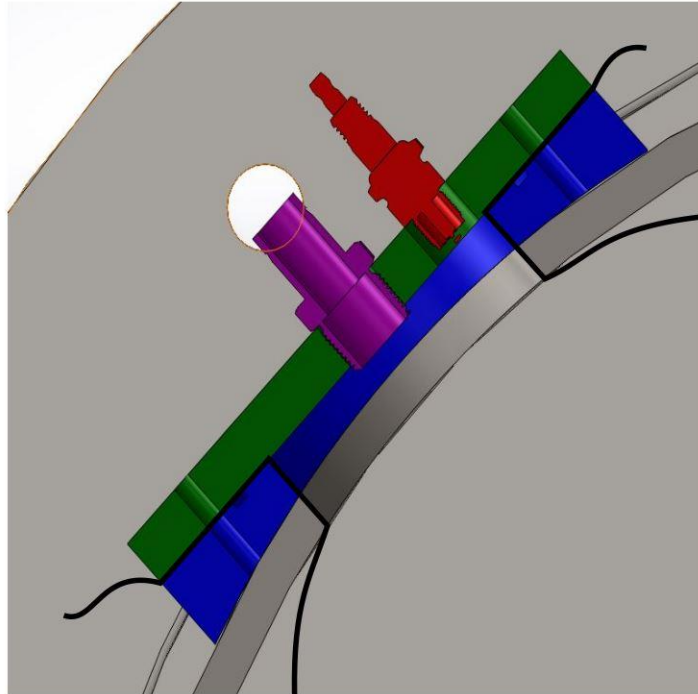the tube-side plate to maintain the seal. Figure 30 shows this setup in greater detail.

Figure 30. Close-up model of explosive bag ignition and filling system.

In addition to the capability to directly initiate detonation with this system, it is useful to have a secondary spark plug located on the side of the chamber for DDT research as well. With spark plugs located at tube end walls, the combustion wave causes gas to expand next to the closed end, allowing a piston-like affect which can alter the acceleration characteristics [30]. The second spark plug can be used to examine this effect as it is located further from the endwall, further increasing the flexibility of the experimental apparatus.

Shock Ignition System

The shock induction system uses the inspection assembly to hold a diaphragm in place so that pressurized inert gas can be used to develop a shock in the reactant gasses in order to induce detonation directly, bypassing the DDT process. The diaphragm is cut from a sheet of polycarbonate, compressed between two O-rings, and burst by a stationary blade affixed to a ring when the correct pressure differential is reached. To make the diaphragm easier to install, it should be cut with holes in the same bolt pattern as the tube flanges, so that it can be slid over the bolts before they are inserted into the opposing flange. After this, the O-rings will compress and hold the diaphragm in place. The blade assembly is shown in Figure 31 and Figure 32.
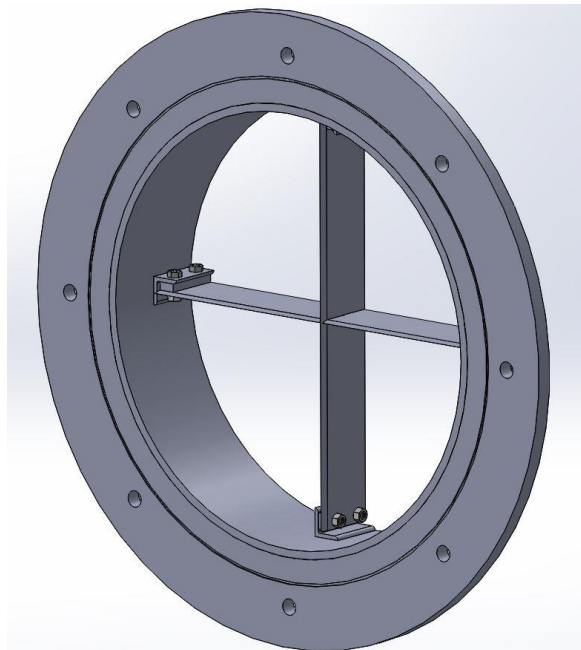

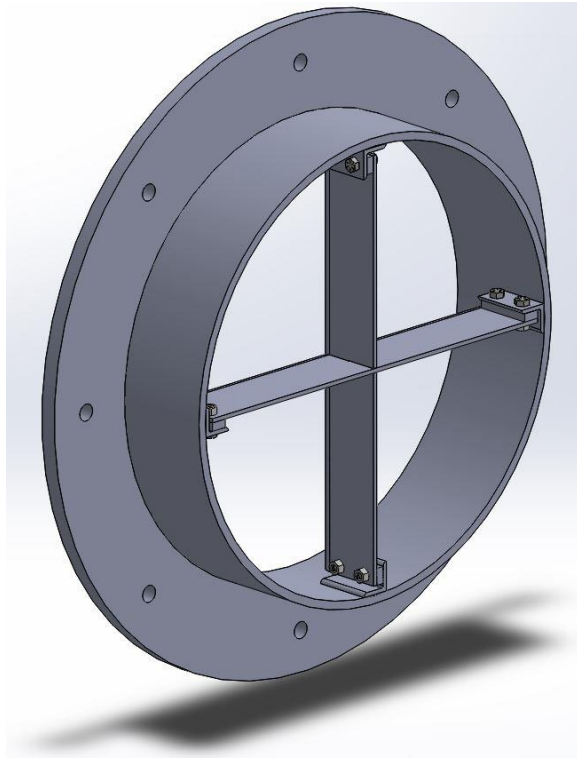**Figure 31. Front view of blade assembly.**

Figure 32. Rear view of blade assembly.

The blade assembly is attached to a short length of tube, itself attached to a flange with the same bolt pattern and O-ring groove as the main tube's flanges. This allows the diaphragm to be compressed between the blade assembly flange and one of the flanges of the main tube. The tube of the blade assembly is narrower than the main tube, enough so that it can be welded to the flange without the weld preventing the flanges from sealing flush against one another. Figure 33 shows the blade assembly (red) installed into the inspection assembly (blue).
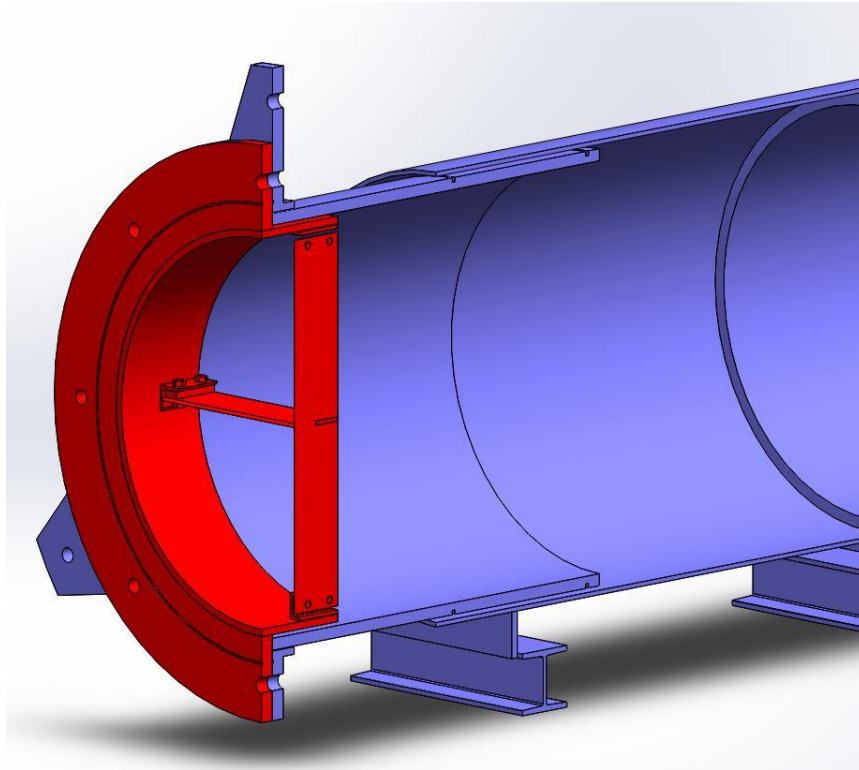
Figure 33. Section view of blade assembly installed in inspection section.

The diaphragm is placed in front of the blade assembly as shown in this image before the internal tube is extended but after the bolts are inserted into the bolt holes from the rear, so that they can be used to hold it in place. This is shown, without the bolts, in Figure 34, with the plastic diaphragm in yellow located on the left side of the blade assembly.
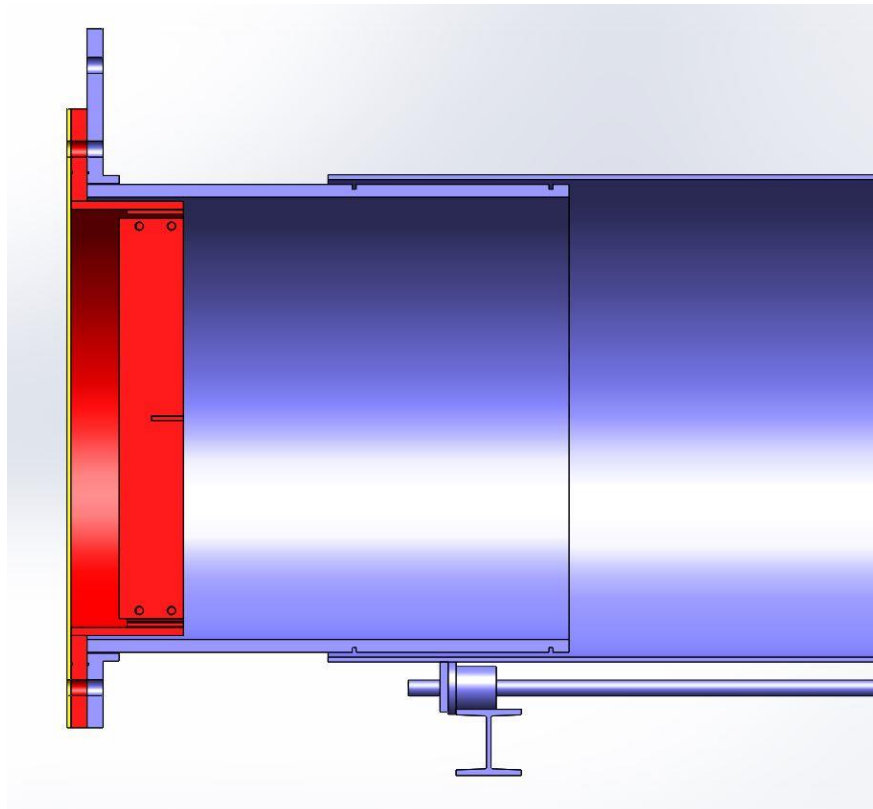
Figure 34. Profile section view of blade assembly installed in inspection assembly.

Alternatively, a metal diaphragm can be used if a stronger shock is required. The metal diaphragm would require bolt holes to ensure that it did not slip from the grip of the O-rings and become a projectile further down the tube, and would need to be scored on both sides to ensure a consistent burst pattern as shown in Figure 35, with a cross pattern extending the length of the internal diameter of the tube, but not reaching the circle compressed by the O-ring, as this could cause the assembly to leak. This should be done with a guided cutting tool or punch to ensure a consistent depth.
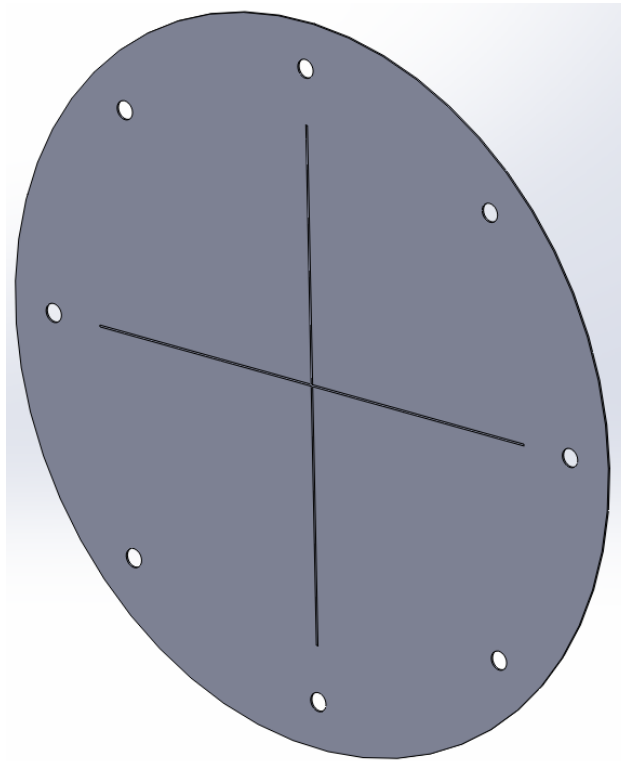
Figure 35. Metallic diaphragm, scored for repeatable bursting behavior.

These metallic diaphragms would not need the cutting blade to burst consistently, and so they could be secured between one of the inspection assembly flanges and the opposing main tube flange.

Diagnostics

The diagnostics consist of pressure transducers and photodiodes that repeat down the length of the tube in addition to the optical systems located near the end of the tube.

Pressure Diagnostics

       The pressure transducers need to be isolated from the tube, as the vibration from the combustion wave will travel through steel at a velocity of roughly 6000 meters per second, reaching the diagnostics much more rapidly than the wave itself.

       To achieve this transducer isolation, a bracket will hold the pressure transducers away from the tube wall and isolate them from vibration with rubber spacers, as shown in Figure 36, with the photodiode assembly in red, the rubber isolators in green, and the pressure transducer in blue. Greater detail on the operation of this device can be found in the Appendix.
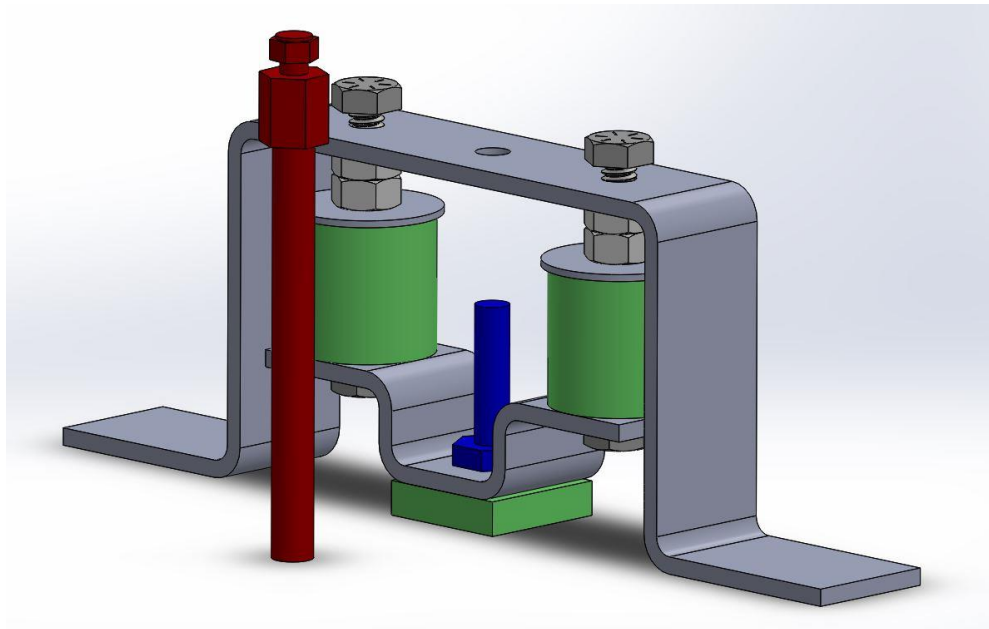

Figure 36. Model of vibration isolation bracket for pressure transducer.

Emission Diagnostics

The photodiodes do not require vibration isolation, but in order to ensure that they only register the emission from the cross section at which they are positioned, they will be mounted on tubes which will distance them from the main body of the detonation tube. This will reduce the likelihood that light emitted further up or down the tube will interfere with the analysis of the shock velocity. These sensors will be used to track the emission of OH* radicals, which are produced during the combustion process, in order to determine the location of the combustion zone independently from the pressure rise.

Schlieren Photography and Planar Laser Induced Fluorescence

Schlieren photography measures density gradients in fluid media, allowing them to be used to visualize fluid flow fields. PLIF analyzes the light generated when a fluid medium is excited by a planar laser, and can be used to characterize fluid velocity, concentration, temperature, or pressure of the fluid in a plane. This would be especially useful for reaction zone studies, as tracking the concentration of OH allows visualization of the reaction zone. The combining of the two techniques allows the reaction zone structure to be studied comprehensively. A simplified diagram of the required setup is shown in Figure 37.
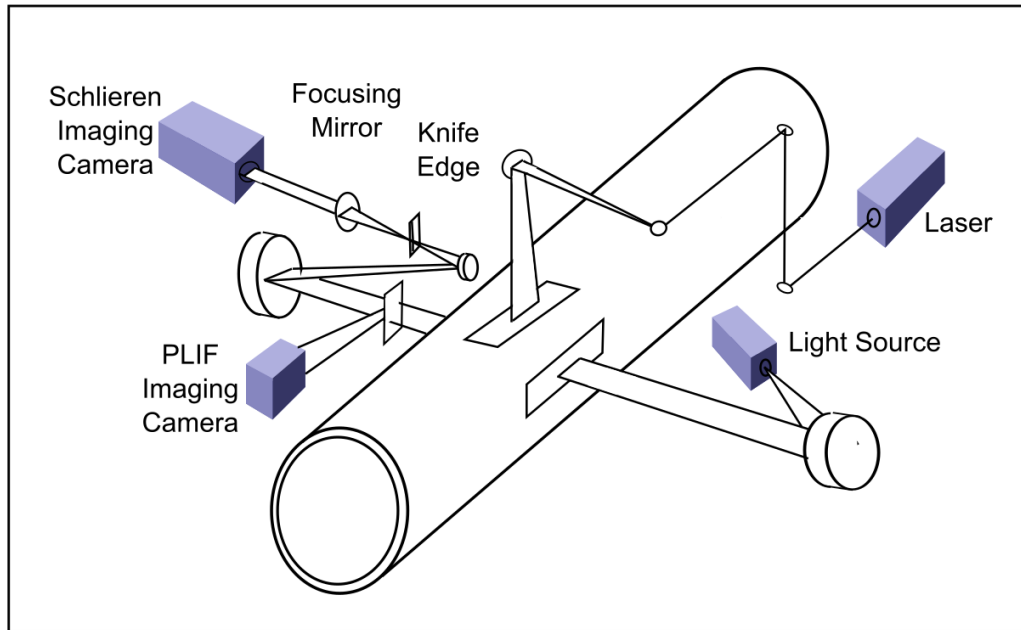
Figure 37. Diagram of PLIF/schlieren imaging combined setup.

Viewing the interior of the tube requires three high-pressure windows, usually constructed from either borosilicate or quartz (fused silica). To enable viewing at multiple stages of combustion wave development, relatively inexpensive round windows will be placed at uniform distances down the length of the tube. The windows themselves will be contained by a cylindrical ring with threaded holes on one side and a face machined to fit the profile of the detonation tube on the other. This will be welded to the exterior of the tube. The window faces will be compressed by one gasket on each side. The hole cut into the tube to allow viewing will be narrower than the window and gaskets, which will be clamped between the tube itself and a bolt ring, as shown in Figure 38.
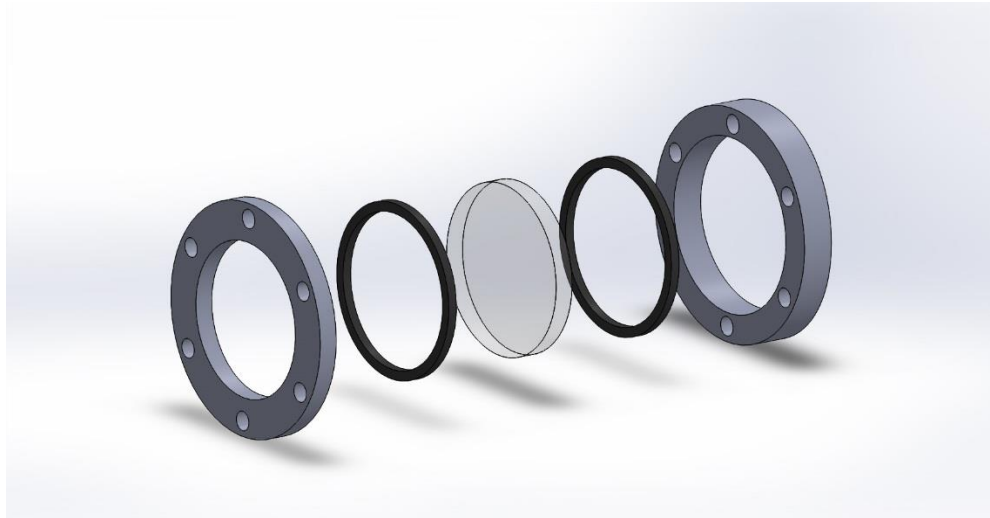
Figure 38. Expanded model of round window.

In order to enable viewing at multiple positions, the final set of windows will be oval, and will operate on a similar principal to the round windows, as can be seen in Figure 39.

Figure 39. Expanded model of oval window.

As before, the rear profile of the threaded window containment must be machined to fit the round profile of the tube, as is demonstrated by the curve on the right side of the sectioned oval window assembly seen in Figure 40. The threads are removed from the image, but the metal casing on the right side is threaded, while the clamp on the left has through-holes.

Figure 40. Profile sectioned view of oval window, showing curve of tube-side attachment.

The minimum thicknesses for the windows were determined for quartz and an aperture diameter of four inches. Both windows, as designed, have a clamped support condition. The round windows were designed with a factor of safety of four, which resulted in a minimum thickness of 14.7 mm. To account for the noncircular shape of the oval windows, the factor of safety was increased to six, resulting in a minimum thickness of 18 mm [31].

Redirection System

The redirection system consists of the ramp, muffler, and mass which are located at the end of the tube. These serve to turn the flow of the combusting mixture upward, to slow it, and to quiet it. This also acts as an additional safety measure in the event that any structural mechanism should fail and allow internal components to be launched from the apparatus. Figure 41 shows the redirection system fully assembled.
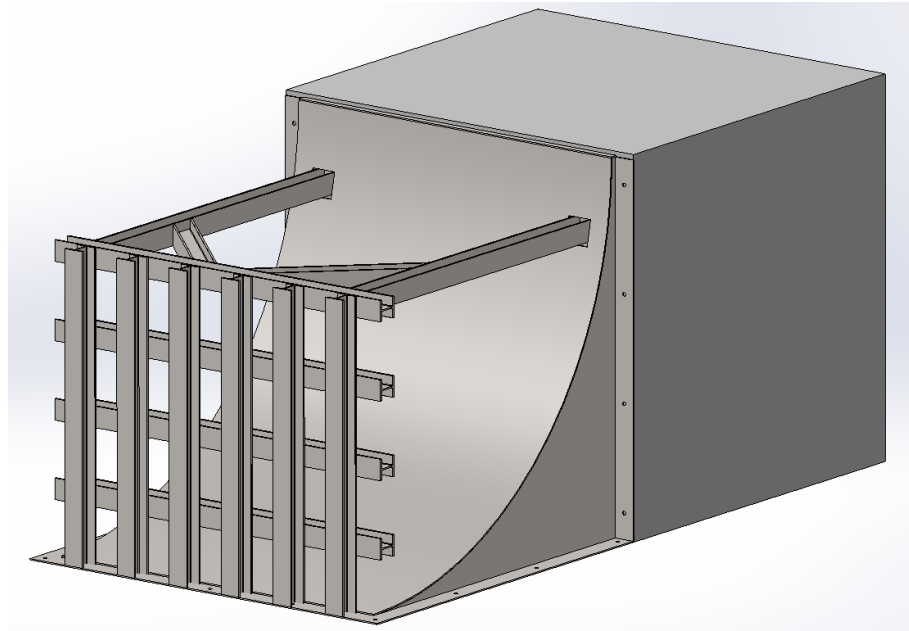
71

Figure 41. Model of exhaust redirection assembly.

The ramp is oversized in comparison to the tube exit in order to increase the effect on any gas that spreads out upon leaving the tube. It is constructed of six metal sheets, the curved ramp which is bent into shape, three laser-cut supports which will assist the ramp in resisting the forces which it will experience during tests, and the two platforms bolted to the concrete foundation below or behind to further assist the assembly in retaining its shape. The mass behind it will be constructed of poured concrete, and will be an extension of the foundation. Figure 42 shows the interior structure of the ramp by removing the rear plate.
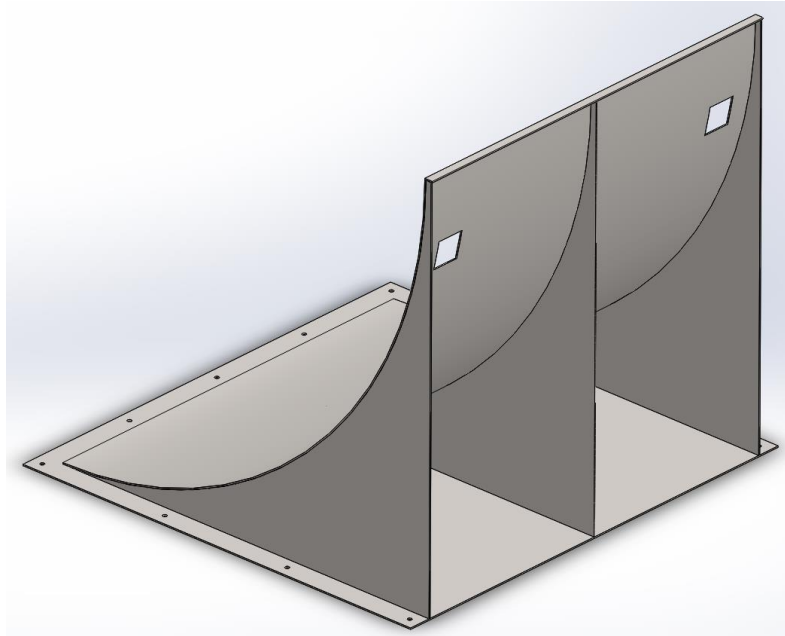
Figure 42. Interior structure of exhaust redirection ramp.

The muffler is constructed from a grid of I-beams. Welded to each other and the bottom of the ramp, they are further constrained by a support system of four additional I-beams, welded to the top of the grid and contacting the support block through slots laser-cut into the ramp before bending. Figure 43 shows the muffler from the rear, with the support beams fully visible.
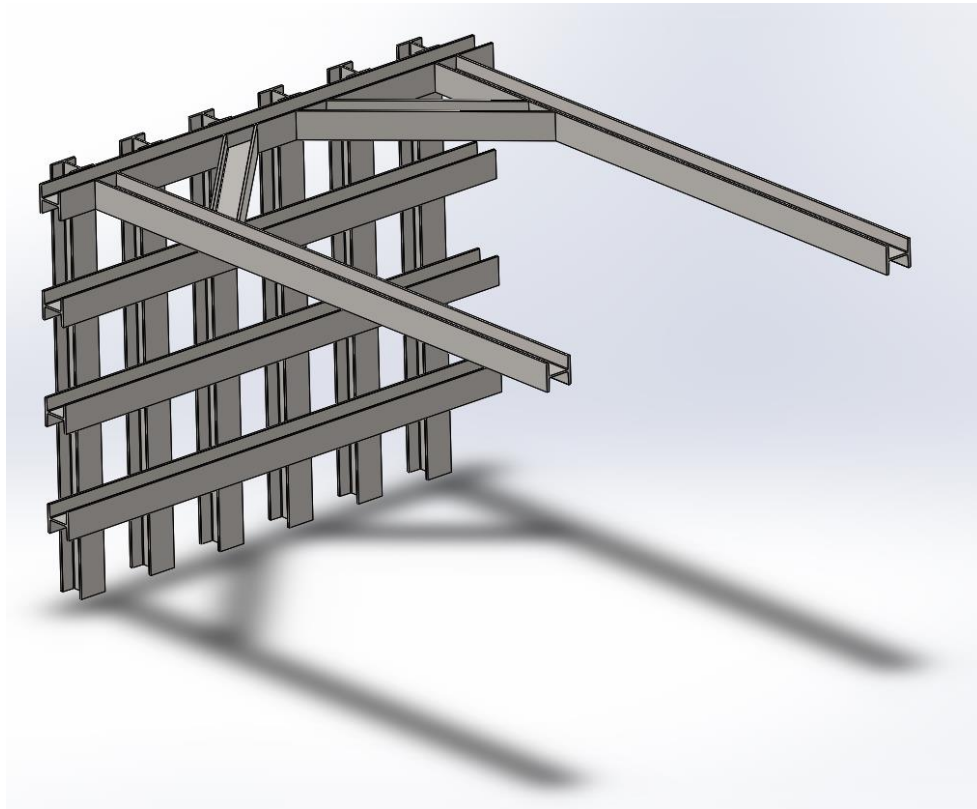
Figure 43. Support beams for redirection system muffler.

Test Procedure

In brief, the end diaphragm would be applied to the tube and compressed, and the researcher would ensure that all bolts were adequately tightened and that the area is clear. A loud warning should be played, notifying any surrounding persons to stay away, and the road nearby the tube end should be temporarily closed off. Any other accessories, such as the internal diaphragm for a direct initiation experiment, should be put in place beforehand.

Before filling starts, all personnel would be located in a safe house area. This room would contain diagnostic and control systems, and the outside would be viewable through a closed circuit camera. Filling valves inside the room would allow the process to be controlled without exposure to the outside facility, and remote operation valves on the circulation system would allow the distribution to be manipulated. Another set of remote valves will allow pipes running to the control room to be separated from the inside of the tube environment.

Once the amount of desired components filled the tube, the mixing system would circulate the explosive mixture to ensure consistency across the length of the facility. With final checks in place, a second, louder alarm would sound and a red light would indicate that a test was imminent. Ignition via the spark plug or explosive pocket would be done remotely through electrical systems, and direct initiation via shock waves would be controlled manually through valves connected to the inert part of the tube.

In the event of a non-ignition, the contents of the tube must be thoroughly vented and negligible concentrations in the atmosphere confirmed before personnel would be allowed to exit the control room.

5. CONCLUSION

There is a pressing need for loss prevention research with a focus on detonation. Vapor cloud explosions, internal pipe detonations, and coal mine explosions have caused major loss of life and damage to property and infrastructure in the course of essential energy industry operations, and the risk of further disasters is significant. While models for detonation formation and damage exist, the multitude of affecting factors make validation and refinement through experimentation a necessity. This requires large-scale detonation facilities, which are rare.

The detonation tube detailed here would be one such facility, 100 meters in length, with an internal diameter of 70 centimeters. Detonation could be initiated directly by explosive bag or inert shock wave, or gradually by spark ignition. The design is modular, with removable sections to enable multiple setups, and would utilize a considerable array of diagnostics, from pressure transducers, photodiodes, and viewing windows spaced down the length of the tube, to more precise PLIF and schlieren imaging acting through elongated windows near the tube end. The location and academic body of Texas A&M University are well-suited for such a facility, which would be capable of unique experimentation due to the rare combination of size, flexibility, and diagnostic equipment.

REFERENCES

[1] Gray, W., 2012, "The impossible explosion," New Scientist, 213(2858), pp. 44-47.

[2] Bradley, D., Chamberlain, G. A., and Drysdale, D. D., 2012, "Large vapour cloud explosions, with particular reference to that at Buncefield," The Royal Society, 370(1960), p. 544.

[3] Johnson, D. M., Tomlin, G. B., and Walker, D. G., 2015, "Detonations and vapor cloud explosions: Why it matters," Journal of Loss Prevention in the Process Industries, 36, pp. 358-364.

[4] Pekalski, A., Puttock, J., and Chynoweth, S., 2015, "Deflagration to detonation transition in a vapour cloud explosion in open but congested space: Large scale test," Journal of Loss Prevention in the Process Industries, 36, pp. 365-370.

[5] Sharma, R. K., Gurjar, B. R., Wate, S. R., Ghuge, S. P., and Agrawal, R., 2013, "Assessment of an accidental vapour cloud explosion: Lessons from the Indian Oil Corporation Ltd. accident at Jaipur, India," Journal of Loss Prevention in the Process Industries, 26, pp. 82-90.

[6] Shepherd, J. E., 2009, "Structural response of piping to internal gas detonation," Journal of Pressure Vessel Technology, 131(3), pp. 31204:031201-31204:031213.

[7] Zipf, J. R. K., Gamezo, V. N., Mohamed, K. M., Oran, E. S., and Kessler, D. A., 2014, "Deflagration-to-detonation transition in natural gas–air mixtures," Combustion and Flame, 161, pp. 2165-2176.

[8] Bartknecht, W., 1981, "Explosions : course, prevention, protection," Berlin : Springer Berlin Heidelberg, 1981.

[9] Nettleton, M. A., 1987, Gaseous Detonations : Their nature, effects and control, Dordrecht : Springer Netherlands, 1987.

[10] Castellanos, D., Lewandowski, A., Diaz, A. n., Mejia, A. F., Carreto, V., Mashuga, C., Rangwala, A. S., Cheng, Z., and Mannan, M. S., 2014, "Influence of particle size and

crystalline level on the efficiency of dust explosion inhibitors," Industrial & Engineering Chemistry Research, 53(28), pp. 11527-11537.

[11] Pasman, H. J., Texas, A., and M, U., 2012, "Why research into explosion mechanisms of flammable clouds is still necessary: Reducing uncertainty will make risk assessment and decision making stronger," Industrial & Engineering Chemistry Research, 51(22), pp. 7628-7635.

[12] Zarei, E., Javad Jafari, M., and Badri, N., 2013, "Risk assessment of vapor cloud explosions in a hydrogen production facility with consequence modeling," Journal of Research in Health Sciences, 13(2), pp. 181-187 187p.

[13] Lee, J. H. S., 2008, "The detonation phenomenon," Cambridge , New York : Cambridge University Press, [2008].

[14] Jackson, S. and Shepherd, J., 2009, "Detonation propagation in a high loss configuration," 22nd International Colloquium on the Dynamics of Explosions and Reactive Systems, 22, pp. 1-23.

[15] Peraldi, O., Knystautas, R., and Lee, J. H., 1988, "Criteria for transition to detonation in tubes," Symposium (International) on Combustion, 21, pp. 1629-1637.

[16] Wang, G., Ma, C., Wang, B., and Lin, Q., 2009, "Direct observations of reaction zone structure in shock-induced ignition of methane air mixture," Chinese Science Bulletin (13).

[17] Pintgen, F., Eckett, C. A., Austin, J. M., and Shepherd, J. E., 2003, "Direct observations of reaction zone structure in propagating detonations," Combustion and Flame, 133, pp. 211-229.

[18] Austin, J. M., Pintgen, F., and Shepherd, J. E., 2005, "Reaction zones in highly unstable detonations," Proceedings of the Combustion Institute, 30, pp. 1849-1857.

[19] Oran, E. S., Gamezo, V. N., and Zipf, R. K., 2015, "Large-scale experiments and absolute detonability of methane/air mixtures," Combustion Science & Technology, 187(1/2), pp. 324-341.

[20] Zipf, J. R. K., Gamezo, V. N., Sapko, M. J., Marchewka, W. P., Mohamed, K. M., Oran, E. S., Kessler, D. A., Weiss, E. S., Addis, J. D., Karnack, F. A., and Sellers, D. D., 2013, "Methane–air detonation experiments at NIOSH Lake Lynn Laboratory," Journal of Loss Prevention in the Process Industries, 26, pp. 295-301.

[21] Williams, F. A., 1965, "Combustion theory," Reading, Mass. : Addison-Wesley Pub. Co., [1965].

[22] Jarosinski, J., and Veyssiere, B., 2009, "Combustion phenomena : selected mechanisms of flame formation, propagation, and extinction," Boca Raton : CRC Press, [2009].

[23] Shchelkin, K. I., and Kirillovich, T. I., 1964, "Gasdynamics of combustion," Baltimore : Mono Book Corp., [1965].

[24] Bychkov, V., and Akkerman, V. y., 2006, "Explosion triggering by an accelerating flame," Physical Review. E, Statistical, Nonlinear, And Soft Matter Physics, 73(6 Pt 2), pp. 066305-066305.

[25] Oran, E. S., and Khokhlov, A. M., 1999, "Deflagrations, hot spots, and the transition to detonation," The Royal Society, p. 3539.

[26] Hansen, O. R., and Johnson, D. M., 2015, "Improved far-field blast predictions from fast deflagrations, DDTs and detonations of vapour clouds using FLACS CFD," Journal of Loss Prevention in the Process Industries, 35, pp. 293-306.

[27] Ciccarelli, G., 2002, "Critical tube measurements at elevated initial mixture temperatures," Combustion Science & Technology, 174(5/6), pp. 173-183.

[28] Gieras, M., Klemens, R., Rarata, G., and Wolański, P., 2006, "Determination of explosion parameters of methane-air mixtures in the chamber of 40dm3 at normal and elevated temperature," Journal of Loss Prevention in the Process Industries, 19, pp. 263-270.

[29] Terao, K., 2007, "Irreversible phenomena : ignitions, combustion, and detonation waves," New York : Springer, [2007].

[30] Blanchard, R., Arndt, D., Grätz, R., and Scheider, S., 2011, "Effect of ignition position on the run-up distance to DDT for hydrogen–air explosions," Journal of Loss Prevention in the Process Industries, 24, pp. 194-199.

[31] Harris, D. C., 1999, Materials for infrared windows and domes : properties and performance, Bellingham, Wash. : SPIE Optical Engineering Press, [1999].

APPENDIX

The vibration isolation system applied to the pressure transducers can be better understood from the examination of Figure 44 and Figure 45.
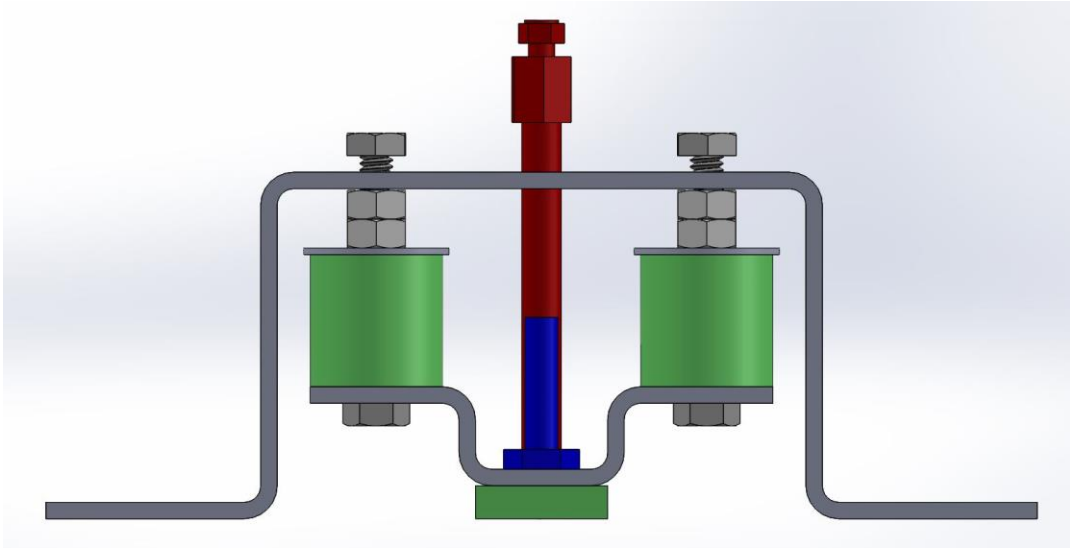
Figure 44. Profile view of vibration isolation bracket
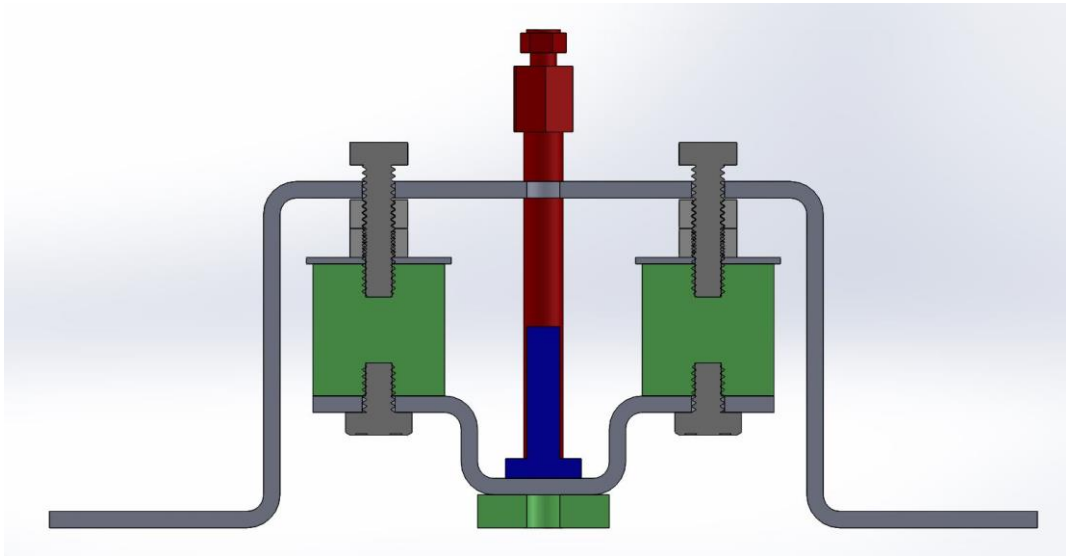
Figure 45. Profile sectioned view of vibration isolation bracket.

To achieve a pressure seal without threading the transducer directly into the tube, the pressure transducer (blue) must be exposed to the gas environment of the tube through the compressed rubber spacer (green) beneath the bracket which it is threaded into, all without metal-on metal contact. In this design, the outer bracket is welded to the tube body. The two upper bolts are threaded through it, as well as through two hex nuts, which are then tightened against one another. The shaft of the bolts passes into the upper rubber spacers (green), ensuring that the rubber spacers do not deform unevenly. The spacers are compressed by wide washers, which are pushed on by the hex nuts as the bolts are tightened. The lower bolts serve to prevent the bottoms of the spacers from slipping from the bracket.
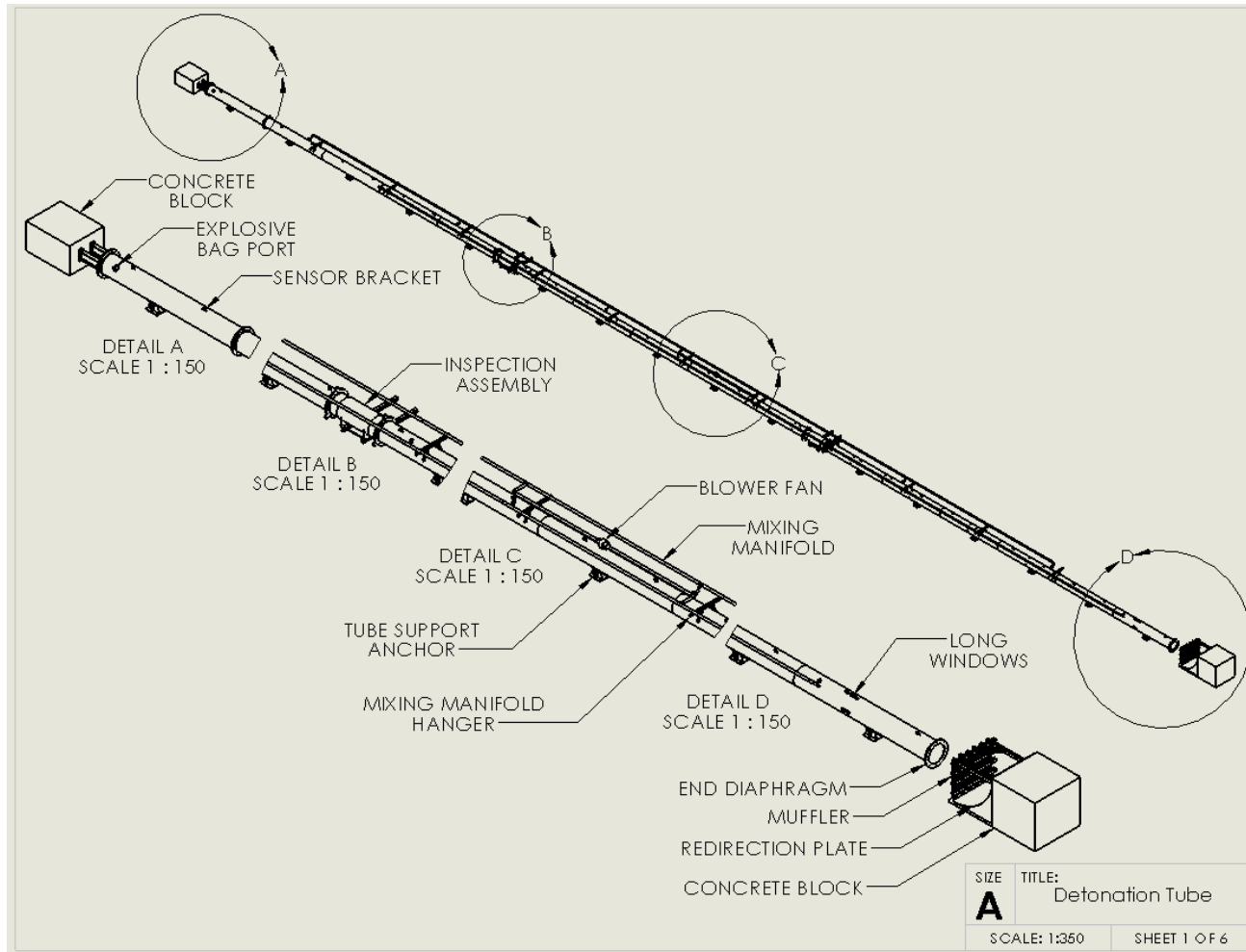
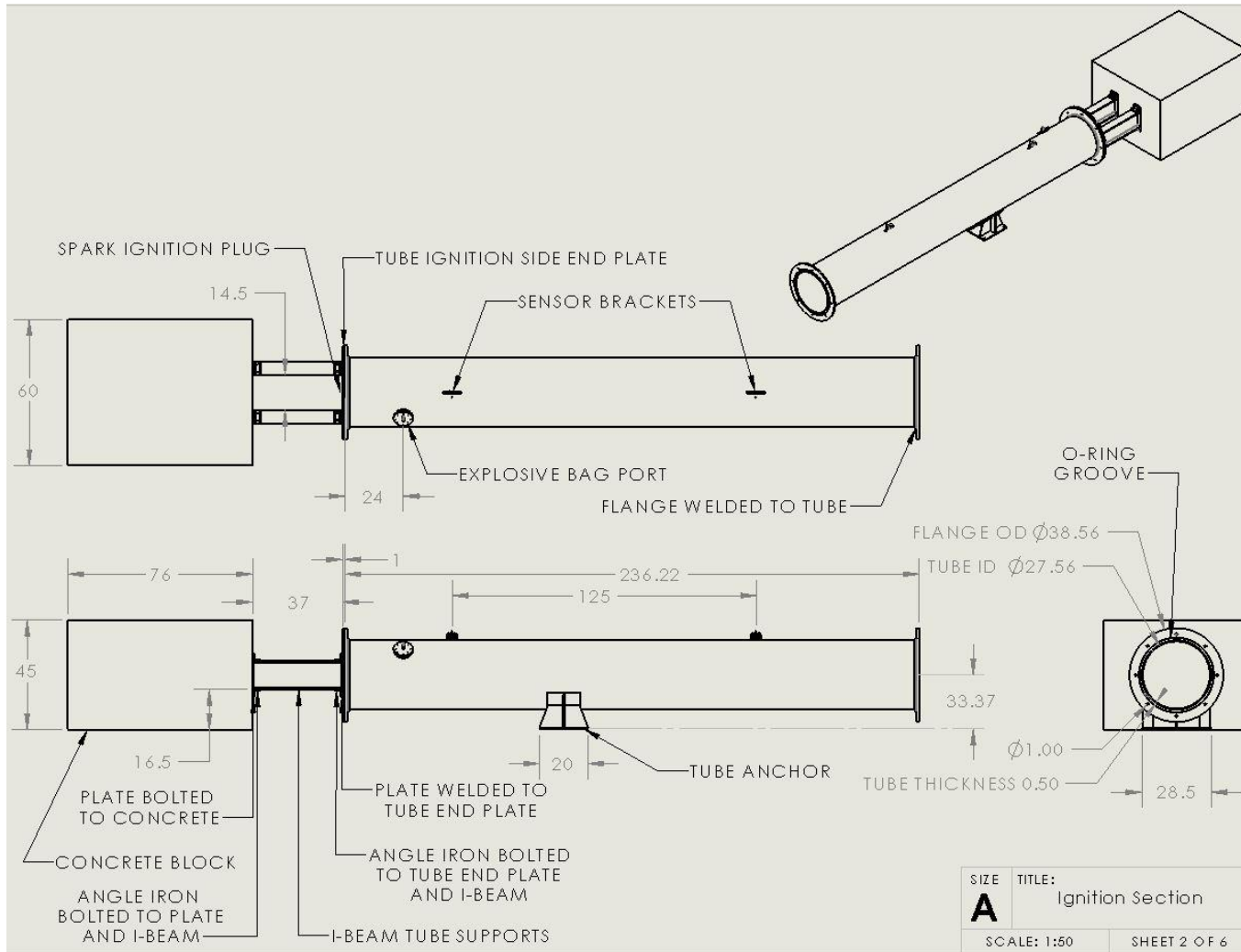**Figure 46. Drawing and layout of detonation tube facility**

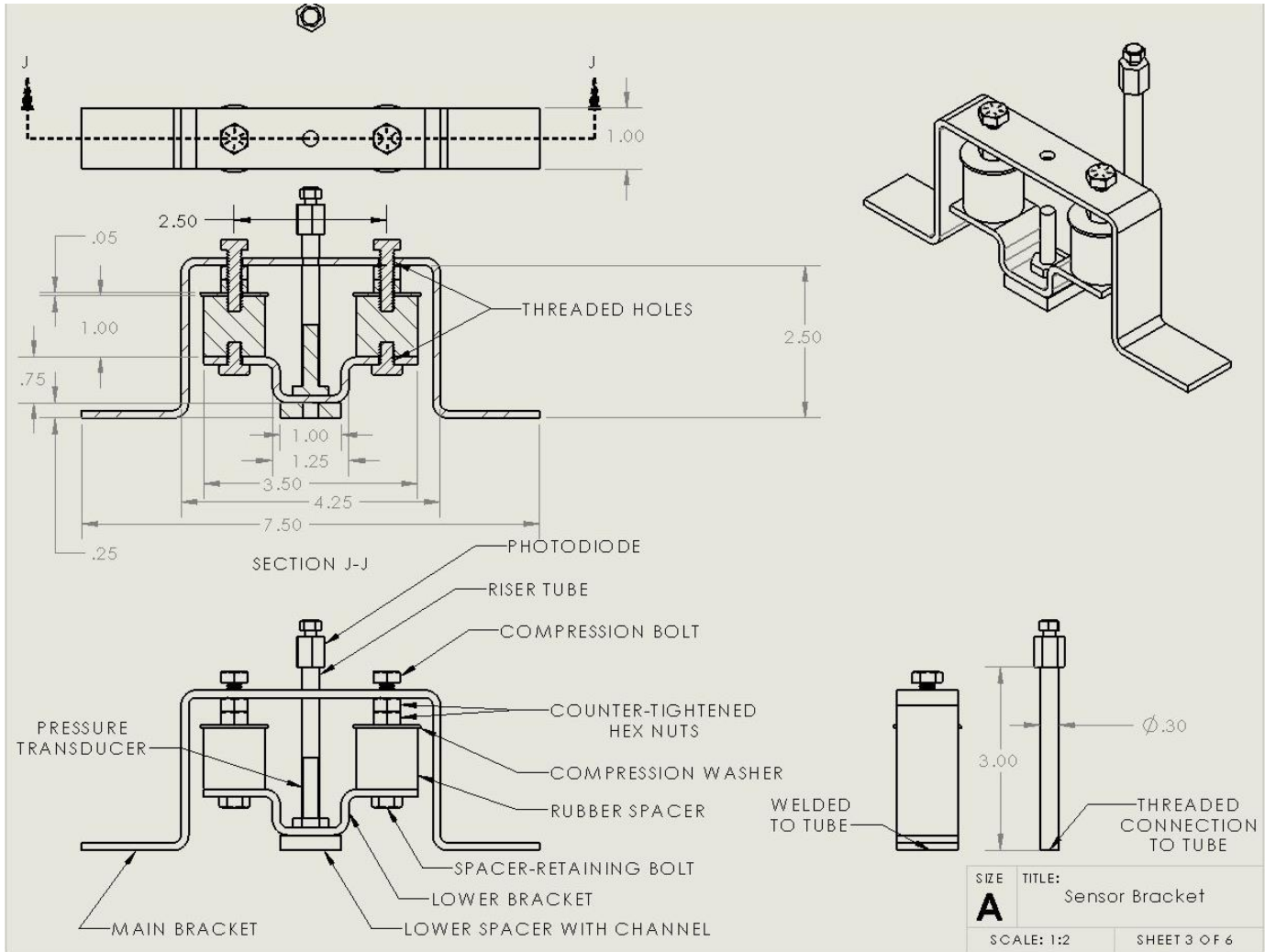**Figure 47. Drawing of ignition assembly and support structure**
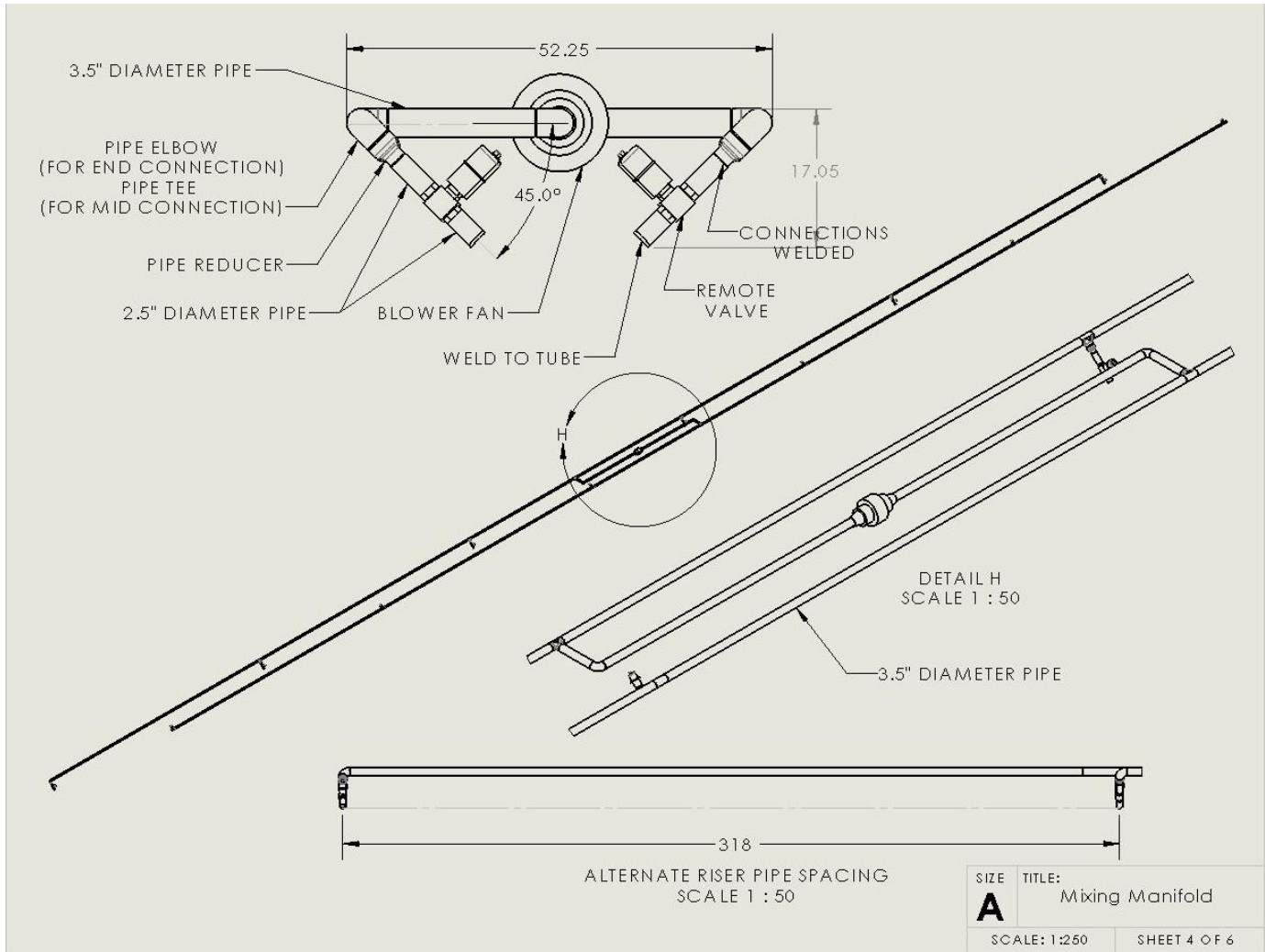
84

Figure 48. Drawing of sensor bracket

85

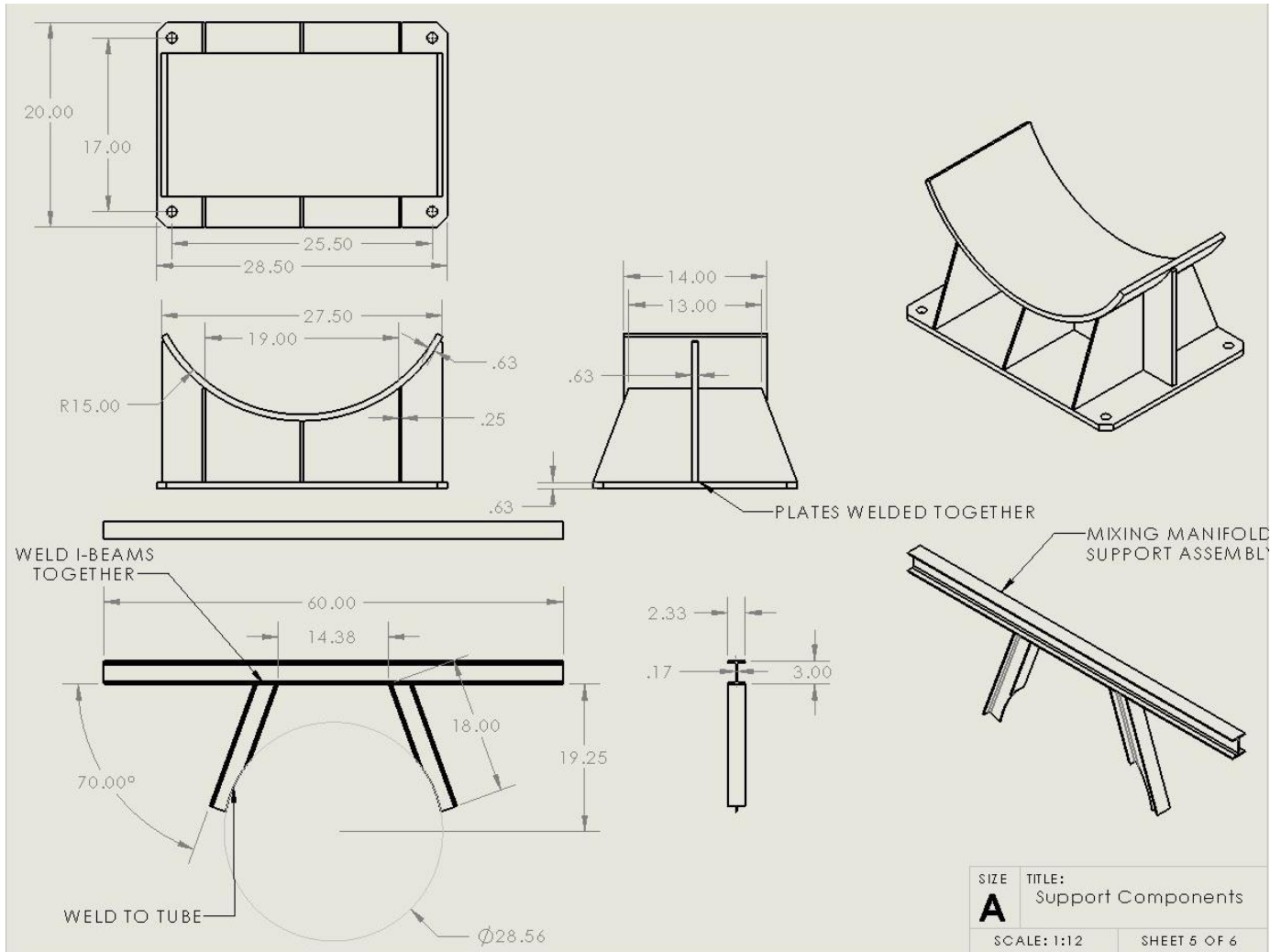**Figure 49. Drawing of mixing manifold**
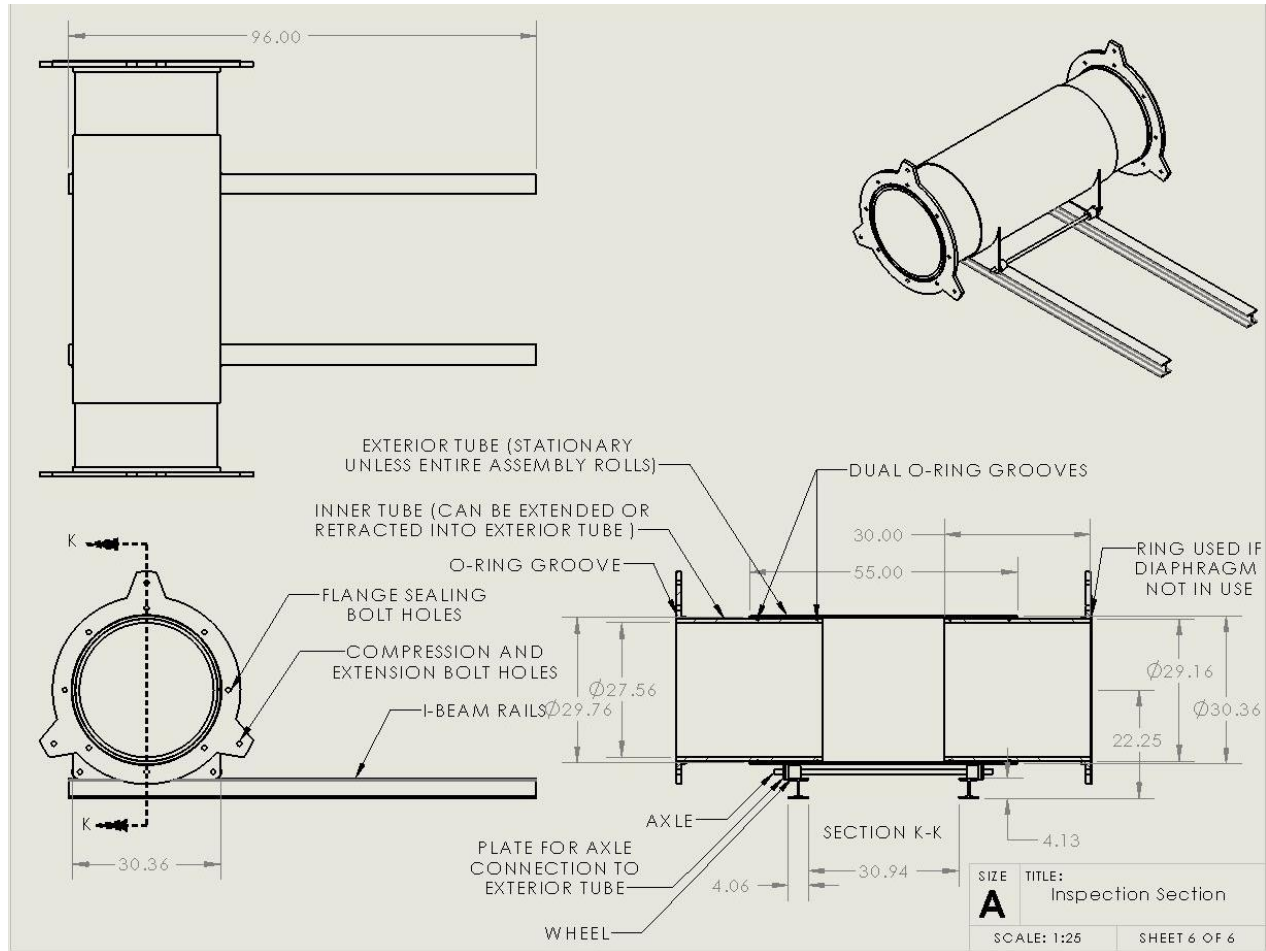
86

Figure 50. Drawing of structural supports

87

Figure 51. Drawing of inspection assembly